



universität
wien



<http://physnano.univie.ac.at>

DISSERTATION

Titel der Dissertation

“Lattice defects in HPT processed fcc
nanometals studied by differential scanning
calorimetry”

angestrebter akademischer Grad

Doktor der Naturwissenschaften (Dr.rer.nat)

| | |
|---|--|
| Verfasser: | Mag. Daria Setman |
| Matrikelnummer: | 9602576 |
| Dissertationsgebiet (lt. Studienblatt): | Physik |
| Betreuer: | Ao. Univ.-Prof. Dr. Michael Zehetbauer |

Wien, April 2010

*for Ildiko
& Dominik*

“Words that do not match deeds are unimportant.”

Ernesto Che Guevarra

Abstract

The current PhD thesis is concerned with the investigation of the nature, distribution and density of lattice defects in nanomaterials which have been processed by Severe Plastic Deformation (SPD). Since these defects have some importance for the exceptional physical properties of SPD nanomaterials, their careful analysis is to enable a better understanding of these properties. As a representative technique for SPD nanostructures, that of High Pressure Torsion (HPT) has been used because of its capability to accurately control strain and hydrostatic pressure. Samples of copper and nickel were deformed by HPT at different hydrostatic pressures to different shear strains, and subjected to different DSC investigations. While in HPT-processed Cu only vacancy agglomerates and dislocations were found, in HPT-processed Ni also single/double vacancies could be observed. The total concentration of vacancies including those of agglomerates was higher, indicating the influence of homologous processing temperature rather than that of stacking fault energy. Generally, the concentrations of all lattice

defects increased with increasing strain and pressure applied. Concerning Ni, additional impurities have shown to stabilize the lattice defects resulting in an increased annealing temperature. Activation enthalpies (Q) were determined by DSC using Kissinger's method.

For Ni, the activation enthalpies of the two annealing peaks were determined as $Q_{vac} = 0.65$ eV and $Q_{disl} = 0.95$ eV, respectively, indicating the annihilation of single or double vacancies, and that of dislocations and vacancy agglomerates, respectively. For the one annealing peak found in HPT Cu, Q amounts from $Q = 0.78$ eV down to 0.48 eV as a function of shear strain applied, in correspondence with the change of peak temperature. Due to the obvious correlation with the strain dependence of external and local internal stresses, the strain dependence of Q , can be attributed to the local internal stresses governing the annihilation of dislocations and/or vacancy agglomerates.

In addition, pure palladium was hydrogenated, subsequently deformed by HPT and analyzed by DSC. For comparison hydrogen-free HPT processed samples were also investigated. The results, for the first time, gave evidence for the formation of vacancy-hydrogen clusters caused by HPT. The vacancy concentration produced in Pd-H by this method is with $7 \cdot 10^{-4}$ extraordinarily high.

Similar to the effect of impurities in Ni, hydrogen seems to stabilize vacancies but also other HPT induced lattice defects as it can be concluded from the increase in peak temperatures and from concomitant observations by transmission electron microscopy.

Kurzfassung

Die vorliegende Dissertation befasst sich mit der Untersuchung der Natur, Anordnung und Dichte der durch Severe Plastic Deformation (SPD) generierten Gitterdefekte in Nanomaterialien. Da diese Defekte in wichtigem Zusammenhang mit den aussergewöhnlichen physikalischen Eigenschaften von SPD Nanomaterialien stehen, ist ihre Analyse für das Verständnis dieser Eigenschaften von grosser Bedeutung. Eine sehr repräsentative SPD Methode ist die Hochdrucktorsion (High Pressure Torsion - HPT), da mit ihr der Verformungsgrad und der hydrostatische Druck kontrolliert eingestellt werden können. In dieser Arbeit wurden Proben von Cu und Ni verschiedener Reinheit mittels HPT bei verschiedenen hydrostatischen Drucken unterschiedlich stark verformt, bevor daran Messungen mittels Differential Scanning Kalorimetrie (DSC) vorgenommen wurden. Während in HPT Cu verformungsinduzierte Leerstellenagglomerate und Versetzungen nachgewiesen wurden, konnten in HPT Ni auch Einfach- bzw. Doppelleerstellen beobachtet werden. Die Gesamtkonzentration an Leerstellen war in Nickel höher als

in Cu, was eher auf den Einfluss der homologen Verformungstemperatur als auf denjenigen der Stapelfehlerenergie zurückzuführen ist. Allgemein nehmen die Konzentrationen der verformungsinduzierten Gitterdefekte mit höherem Verformungsgrad und höherem hydrostatischen Druck zu. Für Ni wurde gezeigt, dass die thermische Stabilität der Gitterdefekte mit zunehmender Verunreinigung zunimmt. Für die Bestimmung der Aktivierungsenthalpien (Q) wurde die Kissinger Methode angewandt.

Die Aktivierungsenthalpien der Peaks in Ni betragen $Q_{vac} = 0.65$ eV und $Q_{disl} = 0.95$ eV, im Einklang mit der Interpretation, dass diese Peaks die Ausheilung von Einzel/ Doppelleerstellen bzw. die von Leerstellenagglomeraten und Versetzungen repräsentieren. Für den einzigen Ausheilpeak in HPT Cu ergibt sich eine Änderung von $Q = 0.78$ eV bis $Q = 0.48$ eV je nach HPT induziertem Verformungsgrad, in Übereinstimmung mit der Variation der Ausheiltemperatur. Da die Grösse der Aktivierungsenthalpie betreffend deren Abhängigkeit vom Verformungsgrad eindeutig mit der Grösse der lokalen inneren Spannungen korreliert, können letztere als Ursache der Änderung der Aktivierungsenthalpien mit dem Verformungsgrad angenommen werden.

Im Rahmen dieser Dissertation wurden auch Pd Proben mit Wasserstoff versetzt und anschliessend einer HPT Verformung bei tiefen Temperaturen unterzogen. Die DSC Untersuchung zeigte die Bildung hoher Konzentrationen von Leerstellen-Wasserstoff Agglomeraten an ($7 \cdot 10^{-4}$), und ausserdem auch die Stabilisierung von Versetzungen mittels Wasserstoff, wie begleitende elektronenmikroskopische Untersuchungen ergeben haben.

Contents

| | | |
|-------|---|----|
| 1 | Introduction | 1 |
| 2 | Aims of research | 5 |
| 3 | Experimental details and theoretical background | 7 |
| 3.1 | Defects in metals | 7 |
| 3.2 | High Pressure Torsion - HPT | 10 |
| 3.3 | Differential Scanning Calorimetry | 11 |
| 3.4 | Hydrogen experiments | 14 |
| 3.5 | Sample preparation | 16 |
| 3.6 | Statistics | 17 |
| 4 | Results and Discussion | 19 |
| 4.1 | Overview | 19 |
| 4.2 | Defects in SPD Metals - [S1] | 24 |
| 4.2.1 | Introduction | 24 |
| 4.2.2 | Experiments | 25 |
| 4.2.3 | Results and Discussion | 28 |
| 4.2.4 | Summary and Conclusions | 38 |

| | | |
|-------|--|----|
| 4.3 | Activation Enthalpies - [S2] | 40 |
| 4.3.1 | Introduction | 40 |
| 4.3.2 | Experiments | 42 |
| 4.3.3 | Results and Discussion | 44 |
| 4.3.4 | Summary | 53 |
| 4.4 | Lattice Defects in Pd - [S3] | 53 |
| 4.4.1 | Introduction | 53 |
| 4.4.2 | Experiments | 54 |
| 4.4.3 | Results and Discussion | 56 |
| 4.4.4 | Summary | 60 |
| 4.5 | Pd with TEM - [S4] | 61 |
| 4.6 | Unpublished results | 69 |
| 5 | Summary & Outlook | 75 |
| 5.1 | Summary | 75 |
| 5.2 | Outlook | 77 |
| 6 | Daria Setman | 89 |
| 6.1 | CV | 89 |
| 6.2 | Publications | 90 |
| 6.3 | Conference contributions | 91 |
| 6.3.1 | Lectures | 91 |
| 6.3.2 | Poster presentations | 93 |
| 6.4 | Cooperations | 94 |
| 6.4.1 | Cooperations within the IC | 94 |
| 6.4.2 | National Cooperations | 94 |
| 6.4.3 | International Cooperations | 95 |
| 6.5 | Teaching | 96 |
| 6.6 | Acknowledgments | 97 |

Introduction

In the last two decades, nanostructured materials revealing a grain size below 100nm have attracted growing interest due to their outstanding properties like increased strength, superplastic behavior, increased magnetic and thermoelectric properties, and sometimes also increased corrosion resistance [1–7]. Two processing strategies have been followed so far for the production of nanostructured materials [8]: bottom-up and top-down methods. With the first method, ultrafine powders consisting of nanostructured particles are processed by different techniques like ball milling and inert gas condensation [9]. Nanostructured films and coatings consisting of nanometer sized grains can also be deposited by vapor phase deposition or electrodeposition [10]. Subsequent warm compression may provide bulk samples but with compromises in grain size and density with poor inter-particle bonding, and easy contamination by impurities. Porosity in particular leads to a marked loss in ductility and fracture toughness. To avoid these problems, one should prefer a top-down method, e.g. starting with a bulk material composed of coarse grains and refining the grains down to the nanometer regime without marked change of the sample shape. Severe plastic deforma-

tion (SPD) [5] seems to be the only technology in the top-down category, but it has a number of variants, including equal-channel angular extrusion (ECAE) [11], accumulative roll-bonding (ARB) [12, 13] and high-pressure torsion (HPT) [14] which have different capabilities in (i) achieving small grain sizes and (ii) to form commercial shape bulk nanostructured materials. It is well known that large strain deformations, for example, by cold rolling or drawing, can result in significant refinement of the microstructure at low temperatures [15]. However, the structures formed are usually such of a cellular type having boundaries with low angle misorientations. At the same time, the nanostructures formed from SPD are ultra fine-grained structures of a granular type containing more than 60% high angle grain boundaries [16]. Formation of such nanostructures could be realized by SPD methods providing very large deformations at relatively low temperatures under the high hydrostatic pressure imposed [1, 11]. Due to the high hydrostatic pressure very high strains can be reached even with constant sample shape. Therefore very high densities of lattice defects are produced [17, 18]. This is especially true for vacancies and vacancy-type defects, which reveal concentrations near to those of vacancies in thermal equilibrium at the melting point [18]. Vacancies have mainly two effects on work hardening [17]. Indirectly they allow edge dislocations to annihilate via climbing increasing the ductility of the material and directly they can form clusters impeding the dislocation motion. Ductility in nanostructured materials was investigated f.e. in [19–21]. High dislocation densities, on the other hand, arrange in cell and finally grain boundaries and therefore produce grains with small sizes. Due to the Hall-Petch relation, the strength of the material increases with decreasing grain size. After rearrangement and particularly annealing of the deformation induced lattice defects at higher temperatures, the increase in strength is lost. Therefore it is important to find possibilities to stabilize these defects and thus gain thermal stability of the enhanced properties. A good solution to this problem is to add

impurities and/or alloying atoms which act as efficient traps for deformation induced defects thus preventing them from annealing [22].

For this work HPT was used as SPD method, as this method revealed to be especially powerful in producing high densities of deformation induced defects and thus a minimum of grain size. This is because of the two-fold effect of enhanced hydrostatic pressure, i.e. (i) to prevent crack formation and thus reveal practically infinite strains (ii) to suppress diffusion and thus annihilation of deformation induced defects. There are several methods for investigation of lattice defects in nanomaterials [23], *direct* ones like transmission electron microscopy (TEM), scanning electron microscopy (SEM) and *indirect* ones like X-ray profile analysis (XPA) [24], residual electrical resistivity (RER) [25], positron annihilation spectroscopy (PAS) [26, 27] and differential scanning calorimetry (DSC) [28]. The latter has been selected for this Ph thesis as it revealed to be an easy and fast technique for investigation of the type and concentration of SPD induced defects and in particular of their thermal stability. Another reason to carry out DSC investigations of SPD processed materials was that these has been done only quite rarely, and that especially for HPT processed nanomaterials practically no papers have been published so far [22, 29].

For this PhD thesis nickel was selected because of the possibility of easily investigating vacancy effects due to their stability at room temperature and the strong influence of impurities [22]. Copper was investigated as a second fcc metal for comparison, not at least because of the significantly lower stacking fault energy. Another reason to select these two metals has been the large knowledge on them thanks to numerous investigations reported in literature but a few only done in HPT processed Ni and Cu. A suitable comparison of HPT specific properties compared to conventionally deformed Ni and Cu, and also to differ-

ently processed Ni and Cu nanometals is therefore possible.

Some calorimetric measurements have been done on hydrogen loaded SPD processed palladium. These studies were made in order to clarify the role of hydrogen for the formation and stability of deformation induced surplus vacancies which have been reported previously to form a high number of very stable hydrogen-vacancy clusters with thermal vacancies provided at high temperatures. Palladium was investigated as one of the most prominent fcc hydrogen storage metals [30, 31].

Aims of research

The aim of this doctoral thesis was to investigate the nature and density of defects in SPD processed metals as a function of hydrostatic pressure and strain. Therefore several questions had to be answered:

- Is it possible to detect lattice defects produced by HPT with DSC?
- Is it possible to distinguish between the different defect types?
- How big is the influence of impurities on thermal stability of defects?
- What is the influence of deformation degree and hydrostatic pressure on the density of HPT defects?
- Is it possible to measure activation enthalpies of deformation induced defects in an accurate way?
- Which parameters do affect the activation enthalpy in SPD deformed nano-metals?

Experimental details and theoretical background

3.1 Defects in metals

All metals chosen in this doctoral thesis are face-centered-cubic (fcc). Fcc is a close packed structure where the lattice atoms are packed as dense as possible (Fig. 3.1).

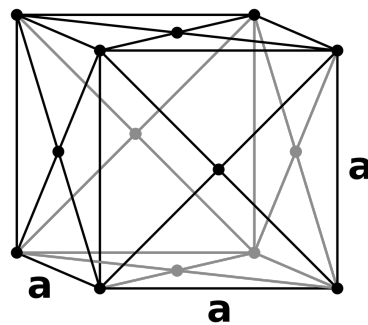


Figure 3.1: The fcc lattice structure.

Crystalline solids have a very regular atomic structure. However, most crystalline materials are not perfect and the regular arrangement is interrupted by

lattice defects. These defects are usually categorized as follows:

0-dimensional: Point defects are defects which are not extended in space in any dimension like vacancies, interstitials and impurities (Fig. 3.2) [32].

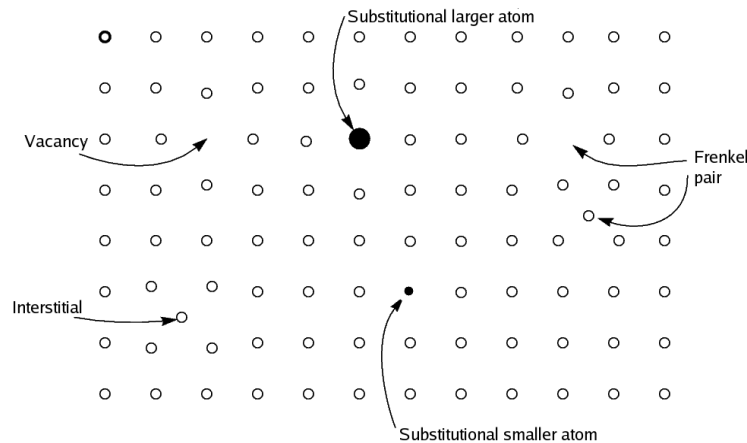


Figure 3.2: Most common point defects in metals.

1-dimensional: Dislocations are linear defects around which some of the atoms of the crystal lattice are misaligned [33]. The presence of dislocation results in lattice strain (distortion). The direction and magnitude of such distortion is expressed in terms of a Burgers vector (b). For an edge type, b is perpendicular to the dislocation line, whereas in the cases of the screw type it is parallel. In metallic materials, b is aligned with close-packed crystallographic directions and its magnitude is equivalent to one interatomic spacing (Fig. 3.3) [34]. It is the presence of dislocations and their ability to move and interact under the influence of stresses induced by external loads that leads to the characteristic deformability of metallic materials.

2-dimensional: Planar defects like stacking faults [33] occur in a number of

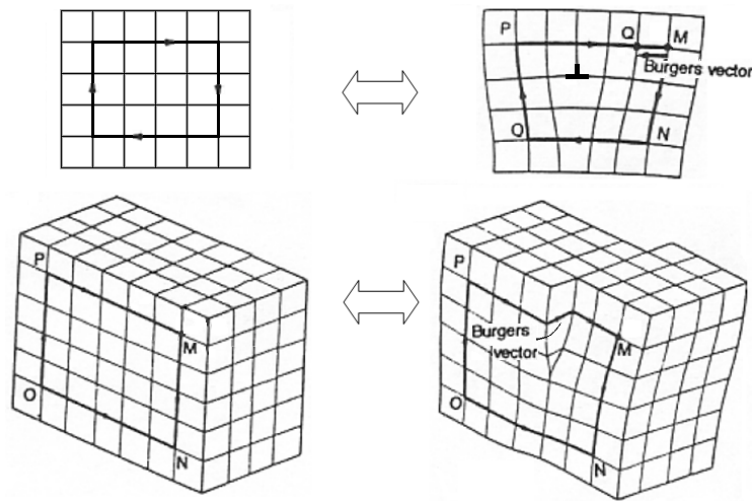


Figure 3.3: Edge and screw dislocations in metals.

crystal structures, but the common example is in close-packed structures. Face-centered cubic (fcc) structures differ from hexagonal close packed (hcp) structures only in stacking order. A stacking fault is a one or two layer interruption in the stacking sequence, for example if the sequence ABCABABCAB were found in an fcc structure.

3-dimensional: Bulk defects are f.e. voids and precipitates.

There are several possibilities to generate defects in metals. Quenching, radiation damage and several types of plastic deformation are the most common. Especially methods of severe plastic deformation (SPD) are of high interest. SPD is a generic term describing a group of metal-working techniques involving very large strains which are imposed without introducing any significant changes in the overall dimensions of the specimen or work-piece. A further defining feature of SPD techniques is that the preservation of shape is achieved due to special tool geometries which prevent the free flow of material and thereby produce a significant hydrostatic pressure. The presence of a high hydrostatic pressure $p \geq 1\text{GPa}$, in combination with large shear strains and not too high processing temperatures

$T \leq 0.3T_m$ (T_m is the melting temperature in K) is essential for producing high densities of crystal lattice defects, particularly dislocations, which results in a significant refinement of the grains [5, 35]. The most common SPD techniques are ECAP (equal channel angular pressing) and HPT (high pressure torsion) and have been schematically presented in Fig. 3.4 [16].

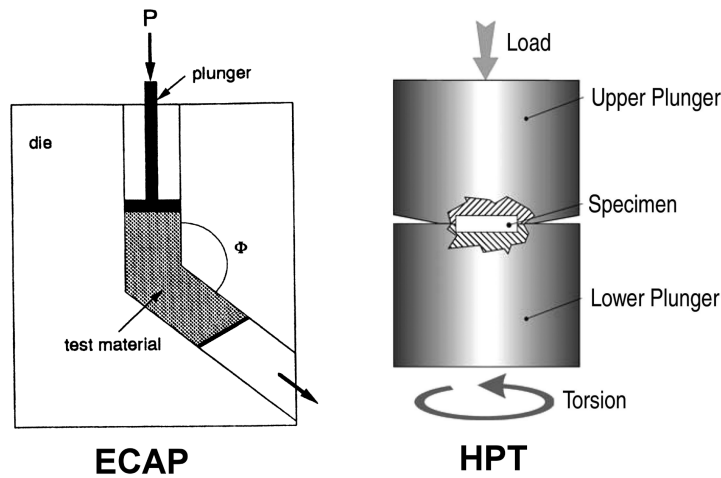


Figure 3.4: Schematic description of ECAP and HPT [16].

3.2 High Pressure Torsion - HPT

For the present doctoral thesis HPT was used as the main processing method for the nanostructured samples needed. HPT refers to a kind of processing in which the sample, generally in the form of a thin disk, is subjected to torsional straining under a high hydrostatic pressure (Fig. 3.4). The disk is located within a cavity in the anvil, a hydrostatic pressure is applied, and plastic torsional straining is achieved by rotation of one of the anvils. The true torsional strain γ is given by $\gamma = r\phi/d$, where r is the distance from the center of the disk, ϕ is the torsional angle in radians, and d is the sample thickness. For comparison with other SPD methods, the true equivalent strain ϵ can be calculated using the re-

lation $\epsilon = (1/a)\gamma$ where the coefficient a takes either the values from a plastic flow criterion (where $a = 2$ for Tresca and $a = \sqrt{3}$ for von Mises) or from the Taylor theory for polycrystals (where $a = 1.65$ for texture free fcc metals and decreases slightly to lower values during continued deformation) [23]. HPT is a very suitable scientific method due to the possibility to control the parameters like hydrostatic pressure, strain and deformation temperature. The 100% dense bulk HPT samples are attractive for products such as nanomagnets with enhanced soft and hard magnetic properties, arterial stents, and devices for micro electromechanical system applications. There have also been recent attempts to scale up the HPT facility in order to process larger bulk samples [36].

For the present work all samples were deformed with the HPT equipment constructed by Pippan et al. at ESI Leoben, Austria [37]. Samples were deformed by applying hydrostatic pressures between 2 - 8 GPa and shear strains of $\gamma = 1$ to 900. Compressive strains resulting from pressure application could be kept below $(d - d_0)/d_0 = 0.1$.

3.3 Differential Scanning Calorimetry

Lattice defects can be observed directly using transmission electron microscopy (TEM), scanning electron microscopy (SEM) and indirectly X-ray profile analysis (XPA) [24], residual electrical resistivity (RER) [25], positron annihilation spectroscopy (PAS) [27] and differential scanning calorimetry (DSC) [28]. In this work most of the investigations of the defect type and concentration in the HPT deformed metals were performed by DSC. DSC measures the energy of the transformation process. The technique of the power compensated DSC is to record the energy needed to establish a zero temperature difference between a substance and a reference material against either time or temperature. During a DSC experiment, a sample is heated over a range of temperature. At some point, the material starts to undergo a chemical or physical change that releases

or absorbs heat. Integration of the area under the heat flow curve yields the enthalpy change associated with the thermal event of interest. Observable processes include simple phase transitions, characterization of polymorphism, and the kinetics and thermochemistry for a variety of complex reactions. A schematic construction of the DSC facility is shown in Fig. 3.5.

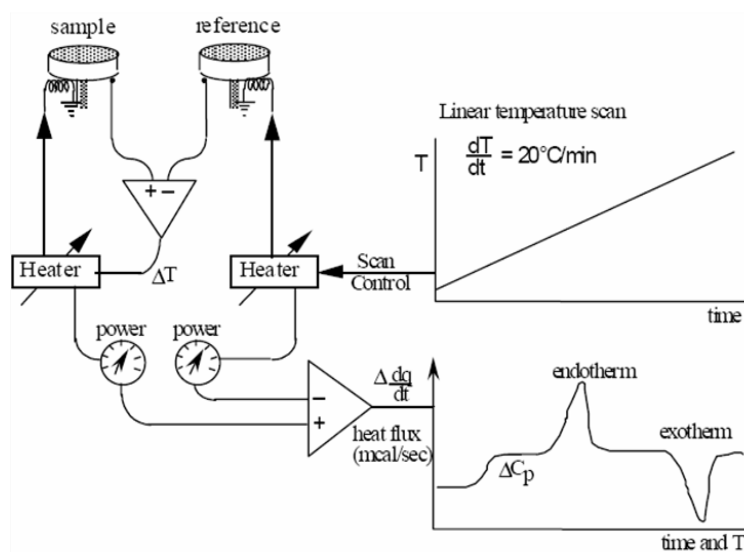


Figure 3.5: Design of typical power compensated differential scanning calorimeter.

As phase transitions result in endothermic peaks, but the annealing of deformation induced defect in exothermic ones, the distinction between these defects is rather easy. The analysis of defect types is possible because different types of deformation induced defects anneal out at different temperatures, due to their different activation enthalpies. The concentration can be directly evaluated from the area of the resulting exothermic peak. The stored energy of dislocations can be related to their density N as follows:

$$E_{stor} = Gb^2 \frac{N}{4\pi\kappa} \ln((b\sqrt{N})^{-1}) \quad (3.1)$$

where G is the shear modulus, b the absolute value of the Burgers vector. κ denotes the arithmetic average of 1 and $(1 - \nu)$, with $\nu = 0.343$ as the Poisson ratio, assuming equal parts of edge and screw dislocations. In equ. 3.1, it is tacitly assumed that the external cut-off radius equals the distance between the dislocations which is not necessarily true for all possible configurations of dislocations. Thus for exact evaluations a configuration parameter α should be added to the argument of the logarithm which may be quantitatively evaluated from TEM or XPA investigations. At any case, it should be noted that the quantity E_{stor} does depend not only on the density and character of the dislocations involved, but also on the arrangement of dislocations, in contrast to the quantity “residual electrical resistivity - RER” described in chapter 4.2.

The concentration of vacancies can be evaluated from the stored energy of vacancies divided by the formation energy ΔH_v^f . In Ni, $\Delta H_v^f = 1.81 \pm 0.02$ eV, in Cu $\Delta H_v^f = 1.21 \pm 0.01$ eV and in Pd $\Delta H_v^f = 1.85 \pm 0.02$ eV per vacancy [38].

Additional information on the nature of the defects can be obtained from the activation enthalpy. For this purpose the method of Kissinger [39] was applied by evaluating the shift of the peak temperature with changing heating rate, as with increasing heating rate the peaks shift to higher temperatures (Fig. 3.6). By plotting

$$\ln \left(\frac{\Phi}{T^2} \right) = -\frac{Q}{RT} + const. \quad (3.2)$$

for various heating rates Φ and absolute peak temperatures T , the activation enthalpy Q can be determined. R is the gas constant.

DSC measurements were performed using Netzsch DSC 204 and Perkin Elmer DSC7. The temperature range from -190°C to 700°C (77K to 970K) and heating rates 0.1 to $100 \text{ K}/\text{min}^{-1}$ were available. The maximum possible sample size was 6 mm in diameter and about in 1.5 mm height. An argon atmosphere helped

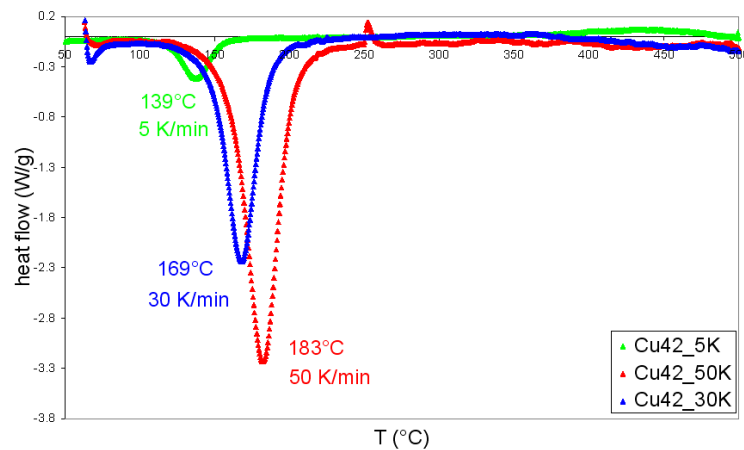


Figure 3.6: DSC - curves for different heating rates of HPT Cu deformed to $\gamma_T = 60$ at 4 GPa

to avoid oxidation of the samples. The minimum peak area to be detected was 0.05 J/g which corresponds to a minimum dislocation density of $N > 3 \cdot 10^{14} m^{-2}$ and minimum vacancy concentration of $c > 3 \cdot 10^{-5}$. This high accuracy can be reached if one uses - as done here with all measurements - the same sample after annealing as a reference

3.4 Hydrogen experiments

In a series of experiments, Fukai and his co-workers [40, 41] showed that in various quenched metal-hydrogen systems vacancies and vacancy agglomerates can be formed in very high concentrations (i.e. up to several %), because they easily get trapped by the hydrogen atoms. In related literature it has been shown these high numbers of vacancies can arrange to even ordered vacancy sublattices [41, 42]. M. Krystian from our research group came up with the idea to try the same experiment with deformation induced vacancies instead of thermal ones. Pd was chosen because this metal has been well known and also well investigated concerning its capability for hydrogen storage. For the deformation, HPT was used in order to achieve a maximum in vacancy concentration. In sum, Pd

samples have been subjected to hydrogen absorption and then processed by HPT at low temperatures. For comparison HPT deformation was performed on pure Pd samples as well.

The samples were loaded in a Sieverts-type (Fig. 3.7) apparatus (build by Dr. Maciej Krystian [43], University of Vienna) resulting in a hydrogen concentration $x=0.6$ (0.6 hydrogen atoms per 1 Pd atom). Special loading conditions slightly above the two-phase region were chosen to avoid internal stresses (Fig. 4.21). The apparatus is based on the volumetric adsorption/desorption technique which is the most important method for determination of kinetics and overall uptake capacity of hydrogen [43].

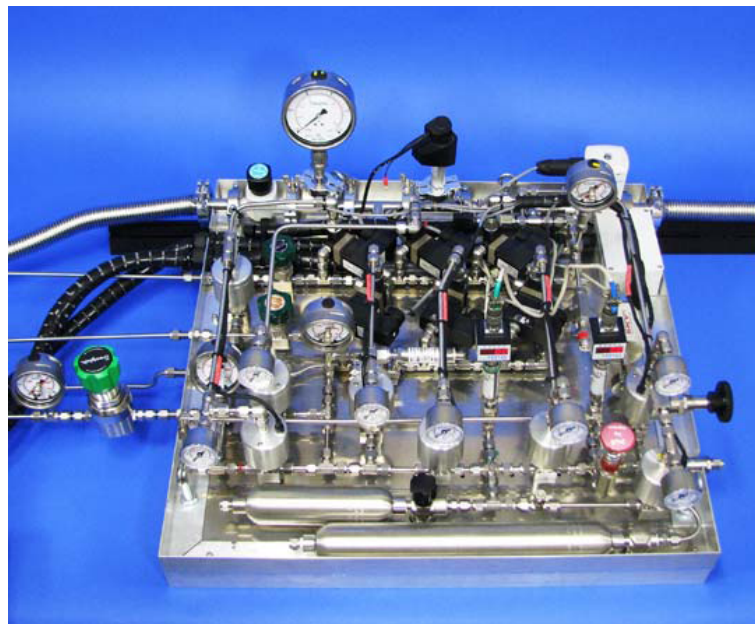


Figure 3.7: View of the main unit of the Sieverts' apparatus (without sample holders) [43]

3.5 Sample preparation

Rods of Pd with 99.95%, Cu 99.99%, Ni 99.998% and Ni 99.99% purity were cut into disks of 6mm diameter and 0.8mm thickness using spark erosion (Charmilles Isopulse Type P25), subsequently cleaned nitric acid (Cu and Ni) or by sandblasting (Pd) and annealed in a Heraeus (Typ ROK 6,5/60) furnace. For Pd a temperature of 1073K for 2h in ultra high vacuum was used. Ni at 913K for 6h and, Cu at 873K for 1 h were annealed in Argon atmosphere.

Afterwards the samples were deformed by HPT using one of the facilities available at the ESI Leoben, Austria [37]. Concerning the deformation hydrostatic pressures of 2 to 8GPa and torsional shear strains of $\gamma = 1$ to 900 were achieved. After the deformation the Cu and Ni samples were cut by spark erosion into discs of 6mm diameter to fit into the DSC crucibles, and cleaned with acetone and nitric acid before DSC measurements. Several samples were cut into rings with an outer diameter of 6mm and 4mm diameter inside for a constant deformation degree. In all cases, the deformation degree was averaged by integration over all radii, resulting in the relation approximation of $\bar{r} = r/\sqrt{3}$.

As concerns the experiments with hydrogen loaded Pd, samples were stored under liquid nitrogen before and after HPT treatment. During HPT processing they were cooled with solid CO₂ pellets ensuring a deformation temperature of 233K (Fig. 3.8). To avoid water condensation during attaching of the cooled sample into the DSC a self-made glove box was installed. The cooled Pd samples were shaped manually in liquid nitrogen with sandpaper into 6mm discs. The weight of each sample was determined with the micro-balance “Sartorius M3P micro” with an accuracy of ± 0.001 mg.



Figure 3.8: CO₂ cooling during HPT deformation.

3.6 Statistics

For this PhD thesis 15 trips to Leoben (Austria) were necessary for HPT deformation of 565 samples altogether. More than 150 hours were spent at the spark erosion machine in 90 sessions for sample preparation. More than 500 samples were measured by DSC. The results were presented on four international conferences. 15 international and national oral presentations and four posters were performed. 8 publications in renowned international journals could be achieved.

Results and Discussion

4.1 Overview

The next chapter describes the work of four main publications which have been already published in international journals [S1-S4]. These publications deal with the questions described in the aims of the present thesis. It is well known that an excessive amount of defects can be produced only in SPD deformed metals. Especially these lattice defects are responsible for the outstanding properties like increased strength. [S1] reports an analysis about the presence and nature of the SPD-induced deformation induced lattice defects. The type and amount is essential for adjusting the requirements for special tasks. The method of Residual Electrical Resistivity (RER) is well known to be a proper method for analysis of vacancies and dislocations although it is suitable rather for the determination of the concentration than the nature of these defects [44].

DSC on the other hand is a less accurate, but easier and much faster technique to determine the defect concentrations, and it is much better suited to identify the nature of defects than RER, via measurement of their activation enthalpy. An-

other important method for characterization of lattice defects is XPA (X-ray line profile analysis). Beside the sizes of CSDs (coherent scattering domain size, that is the size of the largest possible crystalline area without any defect) the absolute value of dislocation densities and give information on the dislocation arrangement [S1]. Since none of the methods is capable to fully quantify the defects alone, only the combination of the methods is capable to do that while benefiting from the specific capabilities of each method. In [S1] and [S2] Cu and Ni samples were deformed by HPT to different strains at several hydrostatic pressures. The annealing of HPT processed *copper* leads to one exothermic peak in the DSC signal which originates from both vacancy agglomerates and dislocations. The separation of these two defects types is possible by applying the XPA method, since XPA is only sensitive to the dislocations. A distinction of dislocations from the total DSC signal is possible by calculating the stored energy corresponding to the dislocation density measured by XPA [S1]. Annealing of HPT processed *nickel*, on the other hand, leads to three annealing peaks (single/double vacancies, vacancy agglomerates and dislocations). The total concentration of vacancies including those of agglomerates was higher in Ni compared to Cu, indicating the influence of homologous processing temperature rather than that of stacking fault energy. Investigating two different purities of Ni (99.99% and 99.998%) gives evidence that impurities trap the deformation induced lattice defects, as the annealing temperatures of the less pure material are higher. Impurities can therefore be used to increase the thermal stability of the nanocrystalline structure. One important parameter governing the defect density available in the SPD materials is the hydrostatic pressure. Samples were deformed at pressures of 2, 4 and 8 GPa for investigation of the role and influence of the applied hydrostatic pressure. With the increase from 2 to 4 GPa leads to an increase of defect density, the hydrostatic pressure of 8 GPa leads to a smaller defect density than 4 GPa caused by recovery during the pressure release after deformation [45].

The second publication [S2] deals with the measurement of *activation enthalpies*. In *nickel* two values of activation enthalpies associated to the annealing peaks could be measured, one for the annealing of dislocations and vacancy agglomerates, and one for the single/double vacancies. Within the accuracy of measurements, they do not vary with strain nor with the pressure applied although the annealing temperatures do (for details see chapter 4.3). The obtained value of the activation enthalpy for the single/double vacancy peak, $Q_{vac} = 0.65$ eV, is about a factor 2 lower than that of vacancy bulk diffusion $Q = 1.18$ eV [38]. This hints at the fact that single/double vacancies move by core diffusion [46, 47]. The activation enthalpy Q for the second peak $Q_{disl} = 0.95$ eV is also lower than the value given for vacancy bulk diffusion, $Q = 1.18$ eV [38]. This indicates that with the mechanism of dislocation annealing deformation induced excess vacancies (-agglomerates) are involved.

The activation enthalpy of *copper* shows a strong decrease with strain. This decrease could be caused by the high vacancy concentration produced by SPD. But as this concentration is very high already at small strains and becomes constant with higher ones, another explanation have been favored. Not only the level of external stress but also that of long range local internal stress measured by XPA show a strain dependence which is strictly symmetric to that of the activation enthalpy. This strongly suggests that internal stresses decrease the activation enthalpy for the motion of dislocations and/or vacancy agglomerates and thus enhance their annealing.

Publications [S3] and [S4] deal with the generation of defects in hydrogenated materials by means of SPD. As already mentioned in the previous chapter, the idea of these experiments was to store high numbers of vacancies through trap-

ping by hydrogen and to provide the surplus vacancies by SPD instead of quenching from high temperatures.

Pd of 99.95% purity was hydrogenated and subsequently processed by HPT to very high torsional strains of about 900 at a hydrostatic pressure as high as 8 GPa. To prevent desorption of hydrogen during deformation, HPT was performed at 233K using solid CO_2 pellets for cooling. For comparison also H₂ loaded but undeformed samples were investigated by DSC.

The experimental results of the previous experiments of Ni [S1, S2] were very helpful as the metals Ni and Pd have similar material parameters (melting point, lattice structure, stacking fault energy, and formation energy of vacancies). In Pd a single/double vacancy peak was found as well as a peak of dislocation annealing [S3]. Comparison of DSC measurements of the deformed with the undeformed state, both after hydrogen loading, showed endothermic peaks of hydrogen desorption. The same peak areas have been observed in both deformed and undeformed samples which indicate that no hydrogen was lost during and after deformation. In the deformed sample, hydrogen desorbs at a slightly lower temperature, as the additional grain boundaries work as fast diffusion paths. The area of the hydrogen desorption peak is about 100 times larger and is superposed to the with the defects' annealing peaks which does not allow a selective evaluation in spite of the fact that hydrogen annealing reveals an endotherm DSC signal in contrast to the exotherm one of defect annealing. Therefore the samples were stored at RT for several weeks to remove the main part of hydrogen. After the desorption of hydrogen an enormous amount of vacancies could be found resulting in a very sharp peak at about 200°C corresponding to a vacancy concentration of $7 \cdot 10^{-4}$. Due to comparison with literature and with HPT deformed, hydrogen free samples it could be concluded that this sharp vacancy peak does not result from single vacancies but mainly from annealing of vacancy-hydrogen clusters; thus, paper [S3] for the first time presented evidence for the formation

of vacancy-hydrogen clusters out of deformation induced vacancies. The dislocation density found in Pd is clearly lower than that measured in Ni, but higher than in comparison to the non hydrogenated Pd-sample, and the annealing has been observed at a temperature being about 150 K higher. This is a clear hint that not only vacancies have been stabilized by hydrogen but also dislocations. These interesting results led to supplementary investigations in [S4].

The publication [S4] comprised a reproduction of the measurements done in [S3] and includes additional TEM investigations for verification of the hints resulting from [S3] concerning the type of defects indicated by the annealing peaks. TEM investigations were performed at first without any thermal treatment, then after a single DSC run up to 523 K and subsequently in situ heated up to 823 K. For the studies by scanning electron microscopy (SEM), the samples after DSC were additionally thermally treated for 1 h at 1073 K under high vacuum in order to allow the vacancies to anneal, i.e. coalesce to pores which could be detected by SEM investigations. These studies demonstrate for the first time that low temperature-HPT of partially hydrogenated palladium allows for the formation of Vac-H clusters even in bulk samples. Hitherto, this formation was only possible in powders [41, 42, 48–52] or thin layers/foils although a very high concentration of voids instead of vacancies was detected [31, 53, 54]. At RT these Vac-H clusters coexist with interstitial hydrogen atoms as well as with monovacancies, and are stable in Pd up to 482 K. To emphasize once more, the results indicate that stabilization by excess H may occur not only for vacancies but also for other deformation-induced lattice defects like dislocations, and/or grain boundaries. Altogether, these facts show that nanometals may experience a marked increase in thermal stability through solute hydrogen.

As publications have to be rather concise there remains not always enough

space for reporting of some results although they may be important. Therefore the most interesting unpublished results made in frame of this PhD thesis have been summarized in the chapter following the presentation of publications [S1-S4].

4.2 The Presence and Nature of Vacancy Type Defects in SPD Nanometals [S1]

4.2.1 Introduction

In the last two decades a few methods for achieving nanocrystalline materials have been developed. Inert gas condensation and consolidation, electrodeposition, ball milling and consolidation, and recently severe plastic deformation (SPD). Although the grains are not always as fine as with the previous methods, SPD offers important advantages like massive as well as 100% dense and pure materials. Moreover, there is a number of features which are not achieved with usually nanocrystallized materials. These are (i) considerable ductility, (ii) changes in phase stability, (iii) enhancement in diffusion. Comparing the nanostructure of SPD-nanomaterials with those achieved by the other methods, it is obvious that deformation-induced lattice defects and the connected local strains are specific for SPD and thus, predestined to explain the features (i)-(iii). This gives motivation to study the effects of their concentration and distribution to the SPD special features in more detail. This paper focuses on the investigation of the number and nature of vacancy type defects in SPD-nanometals as it has been recently done by means of annealing calorimetry and -resistometry [4, 22]. X-ray line profile analysis (XPA) revealed to be necessary for quantifying the dislocation density since vacancy agglomerates and dislocations anneal out at approximately the same temperature. These former results are supplied by new

defect-specific investigations of SPD-deformed Ni of different purities, and will be compared with the previous ones [4, 22] and those from literature [55].

4.2.2 Experiments

Samples and treatment

Rods of Ni with 99,99 and 99.998% purity and Cu 99,99% have been cut into disks of 8mm diameter and 0.8mm thickness using spark erosion and subsequently cleaned and annealed at 640°C for 6 h (Ni) and 600°C for 1 h (Cu) in Argon atmosphere. Then they were deformed by a high pressure torsion (HPT) equipment constructed by Pippan et al. at ESI Leoben, Austria [37]. By applying hydrostatic pressures between 2 - 8 GPa, shear strains of $\gamma = 1$ to 134 have been achieved, with $\gamma = r\phi/d$ where r is the radius and d the thickness of the sample, ϕ is the amount of rotation of the HPT process in radiant. Compressive strains resulting from pressure application could be kept below $(d - d_0/d_0) = 0.1$.

Methods

Differential scanning calorimetry The differential scanning calorimetry (DSC) measurements were performed using two different commercial facilities, i.e. a Netzsch DSC204 and a Perkin Elmer DSC7. Heating has been carried out in a linear way in a temperature range from 25 to 600°C. The standard heating rate was 10K/min, but for the determination of the activation enthalpy additional measurements with heating rates of 5, 20, 30 and 50 K/min were performed. To reach the high calorimetric accuracy of the stored energy determination of less than 1%, an annealed reference sample with identical sample mass (within $\pm 0.01\%$) was used.

During DSC measurements, the annealing of deformation induced defects can be observed by the occurrence of exothermic peaks (Fig. 4.1), the area of the peaks correspond to the total enthalpy of annealing defects, from which their

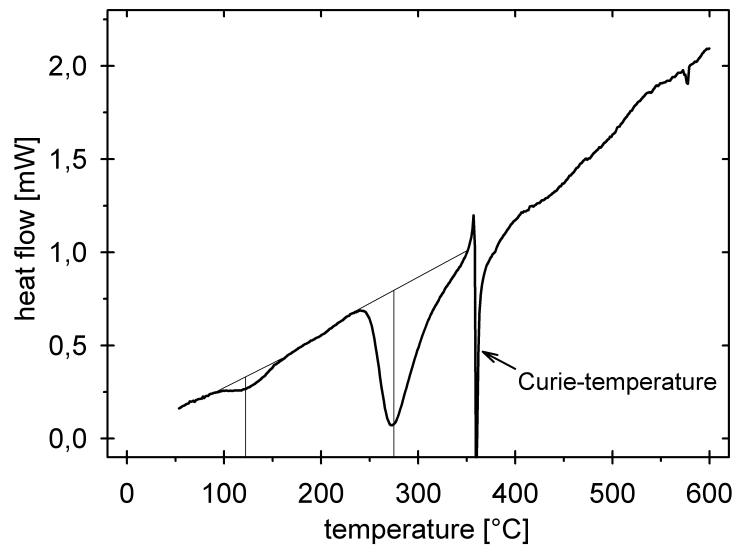


Figure 4.1: A typical heat flow curve as a function of the temperature for HPT-deformed Ni 99.998% exhibits two exothermal peaks. The vertical lines indicate the peak temperatures, the stored energies are evaluated from the integrated areas of the peaks.

densities can be derived (see below). Information on the nature of the defects can be obtained from the peak temperature and the activation enthalpy. For the latter the method of Kissinger [39] was applied by evaluating the shift of the peak temperature with changing heating rate. By plotting

$$\ln\left(\frac{\Phi}{T^2}\right) = -\frac{Q}{RT} + \text{const.} \quad (4.1)$$

for various heating rates Φ and absolute peak temperatures T , the activation enthalpy Q can be determined. R is the gas constant. The stored energy of dislocations can be related to their density N as follows:

$$E_{stor} = Gb^2 \frac{N}{4\pi\kappa} \ln((b\sqrt{N})^{-1}) \quad (4.2)$$

where G is the shear modulus, b the absolute value of the Burgers vector. κ denotes the arithmetic average of 1 and $(1 - \nu)$, with $\nu = 0.343$ as the Poisson

ratio, assuming equal parts of edge and screw dislocations. The concentration of vacancies can be evaluated from the stored energy of vacancies divided by the formation energy ΔH_v^f . In Ni, $\Delta H_v^f = 1.81 \pm 0.02$ eV per vacancy, and in Cu $\Delta H_v^f = 1.21 \pm 0.01$ eV per vacancy [38].

Residual electrical resistivity The residual electrical resistivity (RER) of the deformed samples was measured at liquid helium temperature with the conventional four-wire method. After the final annealing step the geometry factor was determined, allowing for derivation of the defect resistivity $\Delta\rho = \rho(T) - \rho_i$, where ρ_i represents the initial or annealed sample state without deformation and $\rho(T)$ the resistivity after annealing at temperature T [25]. From the HPT pills, 'U'-shaped samples with extra leads for well-defined potential contacts have been cut by spark erosion, the U-shape enabling an approximately constant strain value throughout the sample. The accuracy for measurement of $\Delta\rho$ was better than $\delta(\Delta\rho)/\rho \approx 10^{-3}$, even including repeated re-mounting of samples for annealing purposes. Concerning the evaluation of defect densities, that of dislocations can be derived as $N = \Delta\rho/\rho_{disl}$, where ρ_{disl} denotes the specific dislocation resistivity (being $\rho_{disl} = 2.8 \cdot 10^{-25} \Omega m^{-3}$ for Ni and $\rho_{disl} = 0.8 \cdot 10^{-25} \Omega m^{-3}$ of Cu [56]. If $\Delta\rho$ arises from vacancies, their concentration c_v follows from $c_v = \Delta\rho/\rho_{vac}$, where ρ_{vac} stands for the resistivity per unit vacancy concentration ($\rho_{vac} = 2.9 \cdot 10^{-4} \Omega cm$ for Ni, $\rho_{vac} = 0.62 \cdot 10^{-4} \Omega cm$ for Cu [38]); the values given in parentheses have been averaged from a number of works given in [38, 56].

X-ray line profile analysis (XPA) Selected Ni and Cu samples have been subjected to Multi-reflection X-ray Line Profile Analysis (XPA) using K 1 line of rotating Cu anode generator as well as synchrotron radiation available at the Synchrotron ELETTRA, Trieste, Italy. The wavelength used was $\lambda = 1.54$ nm, the spot size on the sample was about $100 \mu m \times 500 \mu m$. Using a linear position sensitive detector (Braun PSD-50) and a curved one (INEL CPS590), respectively, the

following 6 reflections have been recorded simultaneously: $\{111\}$, $\{200\}$, $\{220\}$, $\{311\}$, $\{222\}$ and $\{400\}$. For details of the diffraction theory of the peak broadening related to domain size see [57, 58], of that related to lattice distortion see [59, 60]. A numerical procedure was used for fitting the Fourier transform of the experimental profiles by the product of the theoretical functions of each, the size and strain Fourier transforms [61, 62].

4.2.3 Results and Discussion

Peak temperature and activation enthalpy

With residual resistivity measurements performed on conventionally deformed samples of Ni 99,998% [17, 63, 64], the two annealing peaks have been identified to originate from the annealing of single and/or double vacancies, and dislocations, respectively. Thus, in the following the peak at the lower temperature will be called "vacancy peak" while the high temperature one will be called "dislocation peak". Fig. 4.2 shows the peak temperatures as a function of strain of numerous measurements on Ni of two different purities which have been deformed by HPT at different hydrostatic pressures. With increasing strain, the dislocation peak shifts to lower temperatures while the temperature of the vacancy peak remains more or less constant. This is a general feature of cold worked materials where the internal stresses connected to the dislocations increase with increasing dislocation density and are assumed to shift the dislocation peak to lower temperatures [65]. As a difference to the dislocations, single and/or double vacancies have a markedly smaller strain field and thus tend to anneal at about a certain temperature irrespective of strain [17]. As concerns the influence of the purity of the material and the applied hydrostatic pressure on the peak temperature, no effect can be seen for the single/double vacancy peak temperatures, whereas the dislocation peaks reveal a moderate dependency.

Performing DSC experiments with different heating rates all defect peaks shift

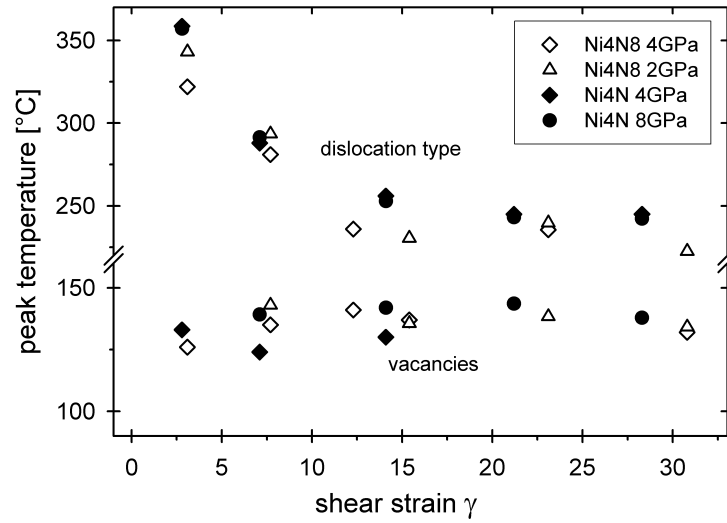


Figure 4.2: The peak temperatures measured by DSC for HPT Ni 99.99% (full symbols) and Ni 99.998% (open symbols) deformed at room temperature at different hydrostatic pressures (see legend) as a function of the applied shear strain. The upper points show the peak temperatures from dislocation-type peak, and the lower ones from the vacancy peak. T_{max} denotes the particular peak temperature. Please note the axis break for better scaling.

to higher temperatures when the heating rate is increased. This effect is used to determine the activation enthalpy according to equation (1) from regression within the Kissinger plot. Fig. 4.3 shows an example for Ni 99.998% which was deformed to a shear strain $\gamma = 7.7$ at a hydrostatic pressure of 4 GPa. The determination of the activation enthalpy of migration Q_{mig} has been performed in differently strained samples results of which are plotted in Fig. 4.4. It can be seen that the values for single/double vacancy annealing lie around 0.65 eV and do not change with strain, which agrees with the strain dependence of peak temperature. The Q_{mig} - values obtained for dislocations amount to about 0.95 eV but, in contrast to the peak temperatures, they obviously do not depend on the strain value at least for strains $\gamma \leq 15$. This problem may be connected with the

fact that the dislocation peak actually consists of two subpeaks, one from dislocations (with varying annealing temperature) and another from vacancy agglomerates (with constant annealing temperature), and that the latter may dominate the first at least in connection with varying heating rates. A support of this idea arises from the fact that the measured activation enthalpy for the second peak $Q_{mig} = 0.95$ eV is lower than that given for vacancy bulk diffusion, $Q_{mig} = 1.18$ eV [38] which is equal to that of dislocation annealing as long as deformation induced vacancies are present. This coexistence of vacancy agglomerates and dislocations is discussed in more detail within the next section.

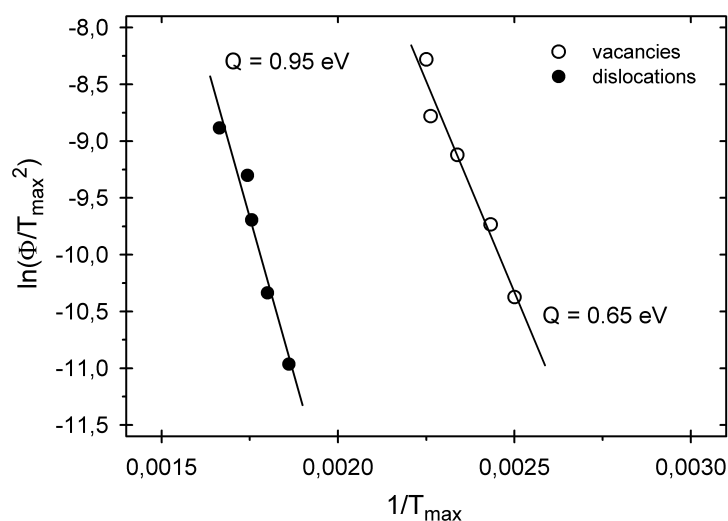


Figure 4.3: Typical Kissinger plots referring to Equ.(1) for vacancy and dislocation peaks measured by DSC, for HPT Ni 99.998% deformed at 4GPa to a shear strain of 8. The full lines represent the regression to the experimental data.

As concerns the value of the activation enthalpy for the single/double vacancy peak, $Q_{mig} = 0.6$ eV, it is about a factor 2 lower than that for vacancy bulk diffusion $Q_{mig} = 1.18$ eV [38] which is typical of the difference of activation

enthalpies of bulk diffusion to that of dislocation core diffusion [46, 47]; thus this mechanism can be assumed to be operative for the single/double vacancies detected here.

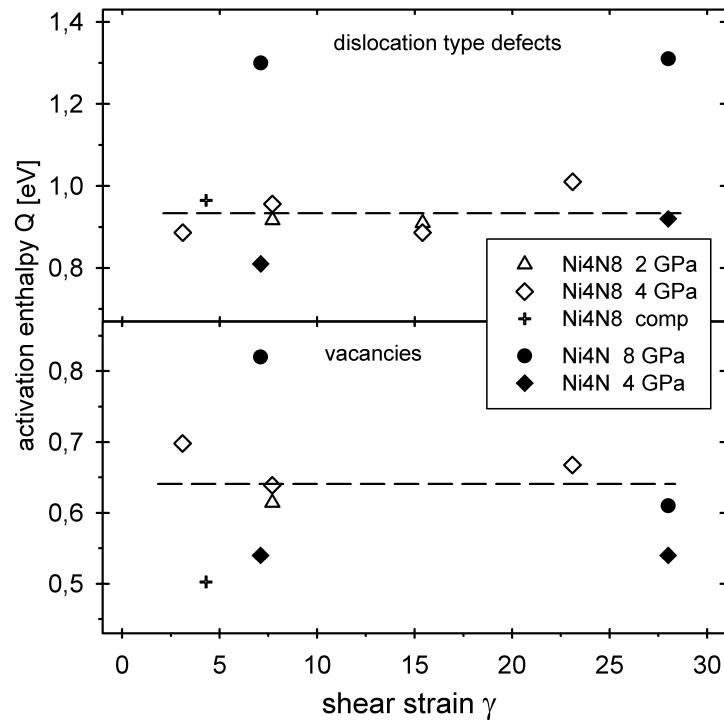


Figure 4.4: Activation enthalpies Q as evaluated from DSC scans, for HPT Ni 99.99% (full symbols) and Ni 99.998% (open symbols) deformed at room temperature at different hydrostatic pressures (see legend), as a function of the applied shear strain. The upper points show the activation enthalpy from the dislocation-type defects and the lower ones from the vacancies. The dashed lines demonstrate rather constant levels of Q . The crosses indicate the values from compression-deformed Ni 99.998%.

Regarding the influence of impurities and the hydrostatic pressure to the activation enthalpies in question, no measurable effect in activation enthalpy neither

from changes in purity nor from those in hydrostatic pressure can be recognized, except the values measured from HPT samples after deformation at a pressure of 8 GPa where Q_{mig} is distinctly higher than with lower pressures. This indicates the formation of a more relaxed, strain less dislocation configuration which may result from static recovery effects which occur during unloading / pressure release after HPT deformation as it has been described in our paper [66] for the case of Cu.

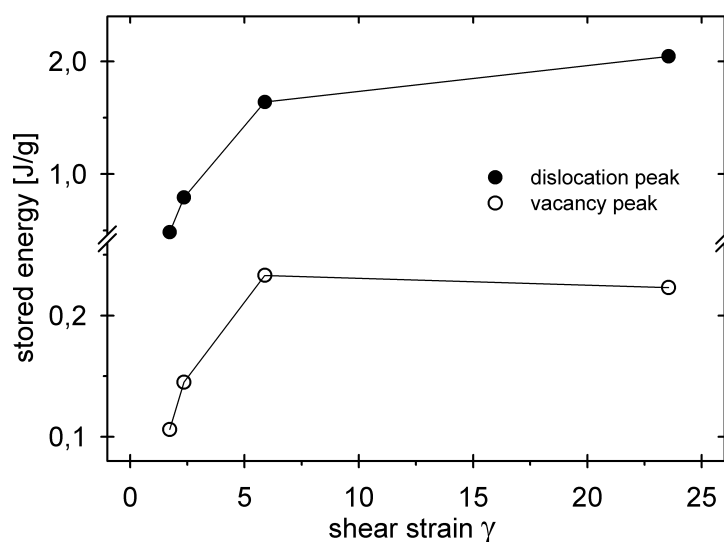


Figure 4.5: Stored energies as measured by DSC of HPT Ni 99.998% deformed at 8 GPa, as a function of the applied shear strain. The lines represent a guide for the eye. Please note the axis break for better scaling.

Stored energy, defect resistivity and defect concentrations

Fig. 4.5 shows the stored energies of the vacancies and the dislocations. A relatively strong increase with strain can be observed both occurring from vacancies as well as from the dislocations. The results of the resistometric measurements obtained by isochronal annealing treatments of HPT deformed Ni samples (at

6GPa hydrostatic pressure) are plotted in Fig. 4.6. Here, two annealing stages are observable: (i) a smooth drop at about 100°C and (ii) a steep drop starting at about 175°C. Stage (i) corresponds to the annealing of vacancies while stage (ii) represent the annealing of dislocations.

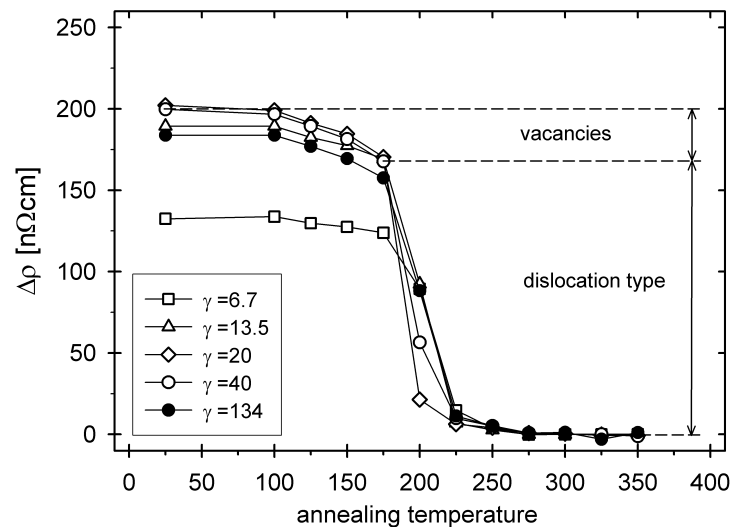


Figure 4.6: Change of the residual electrical resistivity during isochronal annealing of HPT Ni 99.998% deformed at 6 GPa to different amounts of shear strain γ as indicated. The lines represent a guide for the eye. The experimental error lies within the symbol size.

Concentration of single/double vacancies It is easy to evaluate the vacancy concentration from the stored energy as represented by peak 1, by using the formation enthalpy of single vacancies of Ni [38]. Similarly, the vacancy concentration can be determined from the step height of the first drop in Fig. 4.6, using the resistivity contribution per unit concentration of vacancies also given in [38]. In Fig. 4.7 the concentrations of single/double vacancies are presented resulting from evaluating both the data from DSC as well as from RER. Irrespective of the conditions, they all lie in the same order of magnitude of $\approx 10^{-4}$ which

is close to the equilibrium concentration of vacancies at the melting temperature - at least of the metals considered here. A detailed inspection of the graphs shows that below a critical shear strain $\gamma \approx 15$ the concentration of vacancies increases with increasing pressure, whereas with shear strains beyond that value the concentration decreases with increasing pressure. While the behaviour below the critical strain combines with the prediction of Zehetbauer's model to receive enhanced deformation-induced vacancy concentrations at enhanced hydrostatic pressure (i.e. by pressure-induced suppression of vacancy annihilation [18]), the behaviour beyond that strain indicates recovery effects to play a role here: The release of hydrostatic pressure immediately after SPD induces a strain relieving rearrangement of dislocations which is achieved by vacancy-consuming dislocation climb, thus reducing the total vacancy concentration. This explanation is substantiated by previous X-ray measurements of HPT Cu [67] showing that the internal strains markedly decrease beyond critical magnitudes in strain and pressure.

Dislocation density In Fig. 4.8 dislocation densities as function of deformation are presented as they have been evaluated from both quantities, i.e. stored energy and resistivity as it has been described in the experimental section. In addition, dislocation densities as determined by the XPA method are demonstrated. As already reported in paper [67] for the case of SPD Cu, the XPA gives much lower dislocation densities even with the same hydrostatic pressure applied than the other two methods. This discrepancy can be explained by the fact that the broadening of Bragg profiles in the XPA method is only related to dislocation displacement fields which are larger than 5 nm. Smaller pieces of dislocations or, above all, vacancy agglomerates do not affect the XPA signal but will markedly contribute to those of DSC and RER. We can make use of this fact by evaluating the "discrepancy" in terms of concentrations of vacancy agglomerates. Fig. 4.9

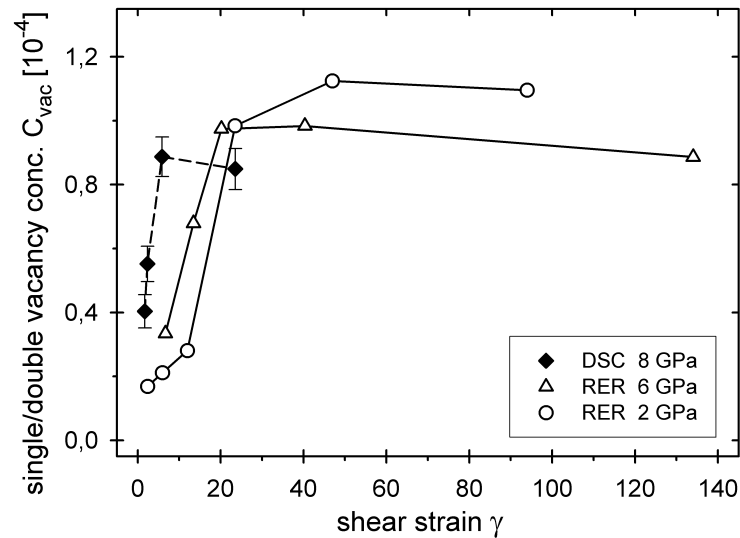


Figure 4.7: The concentration of single/double vacancies evaluated from the first peak/decay of the DSC (full diamonds) and RER (open symbols) measurements of HPT Ni 99.998% deformed at different hydrostatic pressures (see legend), as a function of the applied shear strain. The dashed and full lines represent a guide for the eye. The error bars of the DSC values result from the maximum variation of the literature values for the vacancy formation enthalpy [38] when using them for evaluation of the vacancy concentration.

shows the results of this evaluation exhibiting quite high concentrations of these agglomerates which even exceed those of single/double vacancies by a factor of 4-5. Similar to the single/double vacancies, significantly more defects are stored at higher pressures although they exhibit some enhanced stability i.e. do not anneal so easily with the higher strains and/or pressures applied.

Comparison to HPT deformed copper As already mentioned, a similar investigation has been reported for HPT deformed Cu 99.99% [67]. Pressures applied during HPT amounted to 4 GPa and 8 GPa, and resolved shear strains have been achieved to values beyond 100. The dislocation density has been determined by the XPA method, and the stored energy was measured by DSC in equal way as

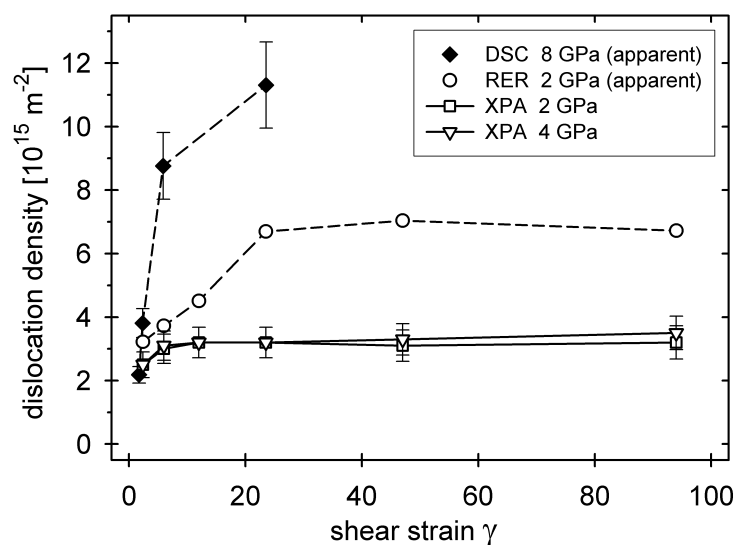


Figure 4.8: The true dislocation density determined by XPA (open up and down triangles), and the apparent dislocation density evaluated from the second peak of the DSC data (full diamonds) or from step height of RER data (open circles), of HPT Ni 99.998% deformed at different hydrostatic pressures (see legend), as a function of the applied shear strain. The dashed and full lines represent guides for the eye. The error bars of the DSC values denote the maximum variation of the literature values for the vacancy formation enthalpy [38] when using them for evaluation of the vacancy concentration. The error bars of the XPA results represent the total error of the method.

described here for Ni. In Cu only one single exothermic peak has been found at temperatures between 180 and 250°C depending on the amount of strain, indicating that this peak must represent the annealing of dislocations produced during HPT. The dislocation density resulting from the measured stored energy is plotted in Fig. 4.10 together with the results of the XPA method. As in case of Ni, a large difference between the results of the two methods is seen which suggests the presence of other defects than dislocations being not detectable by XPA. A similar discrepancy has been found also for ECAP deformed Cu [4]

where this difference has been ascribed to vacancy agglomerates, too. Evaluating the discrepancy in terms of vacancy agglomerates for the actual case of HPT Cu, concentrations of vacancy agglomerates as function of resolved shear strain and hydrostatic pressure were calculated as shown in Fig. 4.11. As in case with ECAPed Cu [4], the vacancy concentration strongly exceeds that of conventional plastic deformation (see dashed-dotted line in Fig. 4.11) which already is an effect of extended hydrostatic pressure and strain being typical of SPD. With further increase of pressure and of strain, the vacancy concentration still increases, although some saturation occurs similarly as in the case of Ni. With respect to the strain this value is reached earlier for the samples deformed at 8 GPa than those at 4 GPa again suggesting some recovery processes being launched through the release of hydrostatic pressure.

Comparing now these results (Fig. 4.11) with those from HPT Ni (Figs 4.7, 4.9) in more detail, it is seen that - with the same strain applied at the same hydrostatic pressure - the total maximum concentration of vacancies considering both agglomerates and single/double vacancies is smaller in Cu than in Ni. For an understanding of this effect, we have to consider the vacancy concentration as a result from the balance of two terms, i.e. of vacancy generation and of vacancy annihilation. While in case of plastic deformation (same amount) the generation term is about the same in Cu and Ni, the annihilation is still governed by the material specific migration enthalpies of vacancies Q_{mig} . For Cu, the latter amounts to $Q_{mig} = 0.76$ eV [38] which is markedly smaller than that for Ni, $Q_{mig} = 1.18$ eV [38]. Therefore it is expected that the total concentration of HPT induced vacancies left after annihilation is lower in HPT Cu than in HPT Ni.

We may also interpret the fact that in Cu no single/double vacancies have been observed, as it was also true for the more impure Ni (less than 99.99%, [22]).

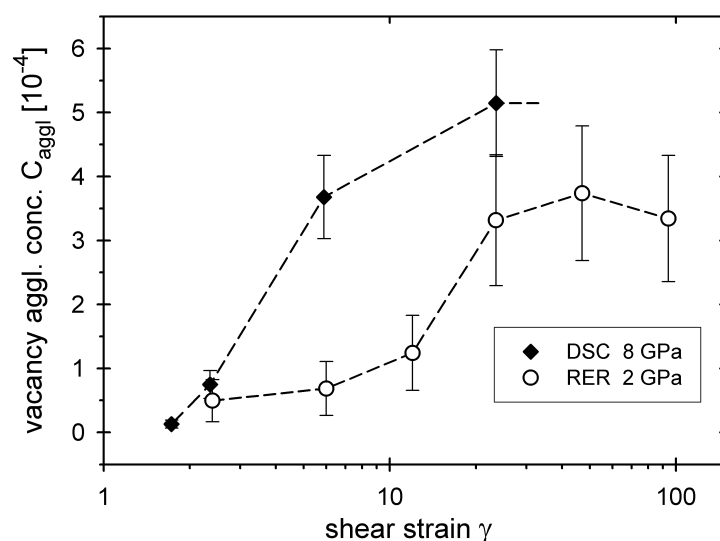


Figure 4.9: The concentration of vacancy agglomerates evaluated from the difference of the second peak of the DSC data (full diamonds) or from step height of RER data (open symbols), and from the results for the true dislocation density, of HPT Ni 99.998% deformed at different hydrostatic pressures (see legend), as a function of the applied shear strain. The dashed lines represent a guide for the eye. The error bars of the DSC as well as the RER values result from the maximum variation of the literature values for the vacancy formation enthalpy [38], and of those for the specific vacancy resistivity.

This fact may be a consequence of the lower stacking fault energy of Cu, and of that of impure Ni (less than 99.99%, [22]) compared with that of very pure one (99.998%): A lower stacking fault energy may facilitate the formation of vacancy agglomerates.

4.2.4 Summary and Conclusions

Two different metals (Ni, Cu) have been investigated with respect to the generation and annihilation of vacancy type defects during and after SPD processing. The combined application of different methods like annealing calorimetry, resistometry and X-ray Bragg profile analysis allowed to specify these defects in sin-

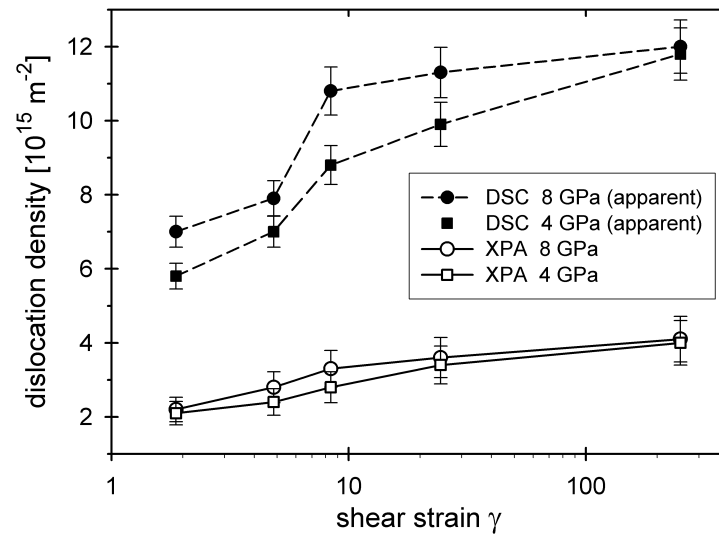


Figure 4.10: The true dislocation density determined by XPA (open symbols) as well as the apparent dislocation density evaluated from the single exothermic peak of the DSC measurements (full symbols) of HPT Cu 99.99% deformed at different hydrostatic pressures (see legend), as a function of the applied shear strain. The dashed and full lines represent a guide for the eye.

gle/double vacancies and vacancy agglomerates, to measure their concentrations and to explore their annihilation mechanisms. The results can be summarized as follows:

1. During SPD processing, very high concentrations of vacancy type defects are achieved being close to those of thermal vacancies at the melting point.
2. Applying increasing plastic deformation and/or hydrostatic pressure, higher concentrations of both single/double vacancies and/or vacancy agglomerates result. The concentration seems to depend on the vacancy migration enthalpy of the material considered, while the nature of the vacancy defects being present appears to be connected with the stacking fault energy.
3. With the highest strains and pressures applied, recovery is launched through

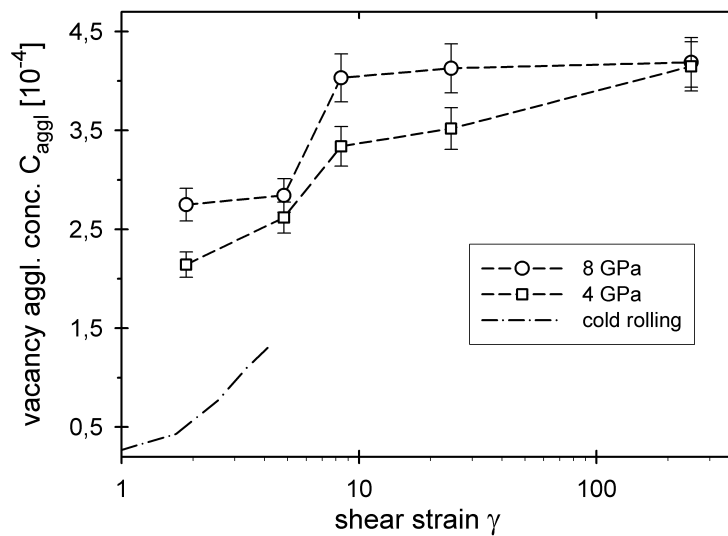


Figure 4.11: The concentration of vacancy agglomerates evaluated from the difference of apparent dislocation density derived from DSC measurements and the values for true dislocation density from XPA measurements, of HPT Cu 99.99% deformed at different hydrostatic pressures (see legend), as a function of the applied shear strain. The dashed lines represent guides for the eye.

the release of pressure after SPD so that the defects - preferably the single/double vacancies - tend to anneal via some core diffusion mechanism. This effect limits or even decreases their maximum possible concentration achieved.

4.3 Activation Enthalpies of deformation induced lattice defects in SPD nanometals measured by Differential Scanning Calorimetry [S2]

4.3.1 Introduction

The enhanced mechanical properties of nano crystalline metals like increased strength are already well known. HPT (high pressure torsion) is a powerful

method of severe plastic deformation (SPD) to gain fully dense samples with a small grain size even below 100 nm. The high deformation degrees reached by SPD methods cause high densities of lattice defects, especially dislocations and thus provide the basis for the formation of new grain boundaries. Details of the produced micro structure have been extensively studied by several papers [2–7, 68]. Unfortunately at least in pure metals the small grains tend to grow already at moderate temperatures, due to advanced annealing of the highly concentrated deformation induced lattice defects which results in a loss of the outstanding mechanical properties. Therefore a careful analysis of the annealing lattice defects and of their annihilation mechanisms is necessary. One possibility is to achieve this by systematic measurements of the activation enthalpies of the lattice defects. First treatises on performing differential scanning calorimetry (DSC) with the method of Kissinger [39] in SPD nano materials proved DSC to be a smart technique for the determination of the activation enthalpy of lattice defects with sufficient reproducibility and reliability [S1].

The present paper focuses on the investigation of the activation enthalpy of the deformation induced defects in fcc metals after HPT deformation. A systematic study of the dependence of the activation enthalpy on both the applied strain as well as on the hydrostatic pressure has been carried out.

The number and nature of lattice defects in SPD-nano metals was recently analyzed by means of annealing calorimetry and resistometry [S1][4, 22]. It was concluded from the specific peak temperatures that the peak at low annealing temperature ($0.23 T_m$, T_m is the melting temperature in K) reflects the annealing of single and/or double vacancies, while that at the higher temperature (i.e. the range of $T = 0.30 - 0.37T_m$) represents the annihilation of both dislocations and vacancy agglomerates. Because of the latter fact, a proper quantification of the defect densities is required to separate the corresponding contributions. X-ray line profile analysis (XPA) is capable to reliably determine dislocations solely

thus enabling such a separation quantitatively. Results from a defect-specific investigation of the annealing behavior of SPD-deformed Cu and Ni are obtained and will be compared to the previous ones [S1][4, 22] and those from literature [55, 69].

4.3.2 Experiments

Samples and treatment

Rods of 99,99% pure Cu and Ni with 99,99 and 99.998% purity were cut into disks of 8 mm diameter and 0.8 mm thickness using spark erosion and subsequently cleaned and annealed at 600° C for 1 h (Cu) and 640° C for 6 h (Ni), respectively, under Argon atmosphere. Afterwards the discs were deformed by high pressure torsion (HPT) at the Erich Schmid Institute Leoben, Austria [37]. Applying hydrostatic pressures of 2, 4 and 8 GPa, the samples were deformed to shear strains of $\gamma_T \approx 1 - 134$. In total more than 75 samples were produced for each material. Here $\gamma_T = (r\phi/d)$ where r , d are the radius and the thickness of the sample respectively, ϕ is the angle of rotation of the HPT process in radian. Any compressive strains resulting from the application of the hydrostatic pressure could be kept below $((d - d_0)/(d_0)) = 0.1$.

Methods

Differential scanning calorimetry The differential scanning calorimetry (DSC) measurements were performed using two different commercial facilities: a Netzsch DSC204 and a Perkin Elmer DSC7. Heating was carried out linearly in a temperature range from 298 to 873 K. For the determination of the activation enthalpy, measurements with heating rates of 5, 10, 20, 30 and 50 K/min were performed. The the peak temperatures were measured with an accuracy of $\pm 0.5K$. Concerning the measurements of the stored energy, an accuracy of less than 1% was achieved, by using annealed reference samples with identical sample masses

(within 0.1%). For the DSC measurements circular samples with diameters 6 mm were cut concentrically from the HPT discs. Each measured stored energy and/or activation enthalpy was associated to a 'mean' representative strain of the sample which has been averaged by integration over the whole sample area. The DSC samples used in the present experiments were discs of 6 mm radius cut out of the HPT-discs concentrically via spark-erosion. The number of defects measured is therefore the integral amount over the whole sample. In order to correlate this to a certain amount of deformation, the torsional shear strain was equally averaged and was used in all plots. During DSC measurements, the annealing of deformation induced defects can be observed by the occurrence of exothermic peaks. The area of these peaks corresponds to the total formation enthalpy of the annealing defects, from which their densities can be derived [S1]. Information on the nature of the defects can be obtained from the temperature of the peak maximum (determined with an error $< 0.5\%$), as well as from the activation enthalpy. For the latter the method of Kissinger [39] was applied in the present paper, by evaluating the shift of the peak temperature for different heating rates: Plotting

$$\ln \left(\frac{\Phi}{T^2} \right) = -\frac{Q}{RT} + \text{const.} \quad (4.3)$$

for various heating rates Φ and absolute peak temperatures T , the activation enthalpy Q can be determined (R is the gas constant).

X-ray line profile analysis (XPA) X-ray line profile analysis is a powerful tool in the analysis of ultra-fine grained and nano-crystalline materials. It provides valuable physical micro-structural parameters such as the density of dislocations and their arrangement, as well as the size and the distribution of the coherently scattering domains (CSD-size) [62]. In certain cases it is also possible to obtain information about the internal residual stresses present in the material by using the method described in [70].

The necessary X-ray data were collected using a highly monochromatic X-ray

beam in the home laboratory, achieved by a special Siemens M18XHF rotating Cu anode generator with a Ge single crystal monochromator. The resulting Cu $K\alpha_1$ radiation was monochromatic with $\delta\lambda/\lambda < 10^{-4}$ and the spot size on the sample was about $100 \times 500 \mu\text{m}^2$. The $\{111\}$, $\{200\}$, $\{220\}$, $\{311\}$, $\{222\}$, $\{400\}$ and $\{331\}$ Bragg reflections were recorded using a linear position sensitive detector Braun PSD-50. The peaks showed asymmetric broadening that was attributed to long range internal stresses and was evaluated according to the procedure described in [70]. Some results of this investigation were already published in a previous paper [66].

Thanks to the fact that XPA is not sensitive to dislocations with a length smaller than about 3 nm, it could be used to separate the shares of the dislocations and the vacancy agglomerates when they contributed to the same DSC peak (see Figs 4.17 and 4.18a); for a close description of the procedure see [S1][4, 39]). For this purpose selected Cu samples were subjected to the Multiple Whole Profile (MWP) fitting procedure [61, 62]. This yields, most notably, the absolute values of the dislocation densities present in the material.

4.3.3 Results and Discussion

Activation Enthalpies

As it should occur with the Kissinger method used with DSC, all defect annealing peaks shift to higher temperatures when the heating rate is increased. According to equation (4.3) the activation enthalpy is determined via a linear regression within the Kissinger plot, as it has been visualized in Fig. 4.13 for the case of Ni. The error for Q from the regression was less than 5% in all cases. The activation enthalpies from DSC measurements of HPT deformed Cu are shown in Fig. 4.12 for different strains and different hydrostatic pressures. The graphs of activation enthalpies exhibit a dependence of Q on the strain *and* the pressure applied, with Q values between 0.78 and 0.48 eV.

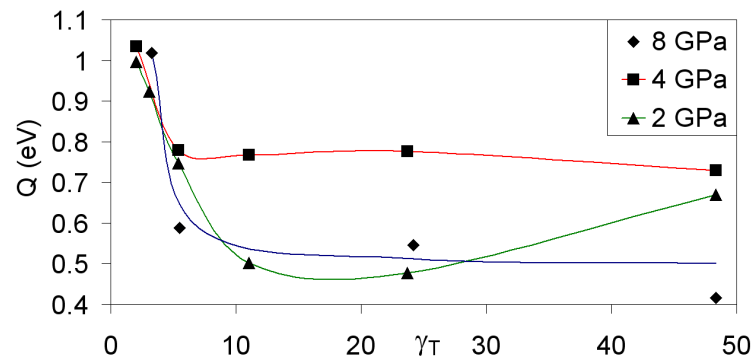


Figure 4.12: The activation enthalpy of Cu as a function of the shear strain for 2, 4 and 8 GPa

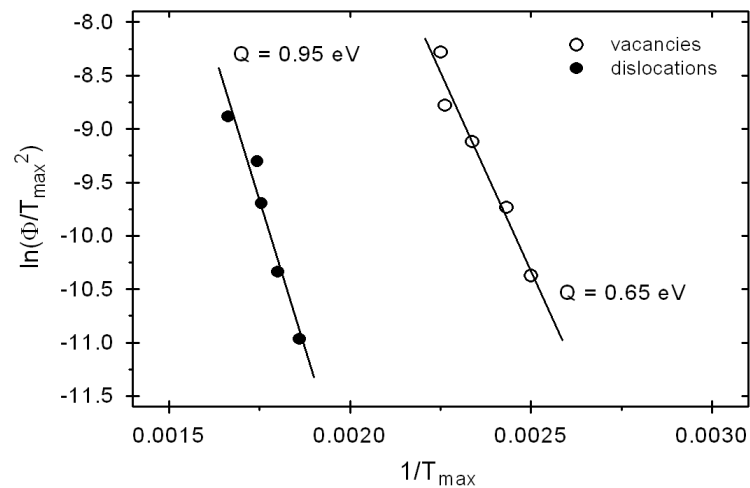


Figure 4.13: An exemplary Kissinger plot for HPT Ni 99.998% deformed to a shear strain of 7.7 at 4 GPa

As concerns HPT Ni, the procedure shown in Figure 4.13 was performed for all differently strained samples. The corresponding results are plotted in Figure 4.14. In contrast to the case of Cu, DSC in HPT Ni revealed two peaks [S1][22], with activation enthalpies $Q(vac) = 0.65 \text{ eV}$ for the single/double vacancies at low temperature one, and $Q(disl) = 0.95 \text{ eV}$ for a mixture of vacancy agglomerates and dislocations at high temperature. These values have been found to neither change with strain nor with the pressure applied nor with the purity of the material.

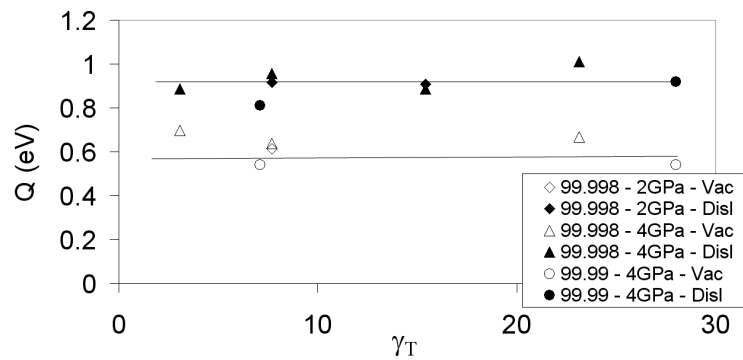


Figure 4.14: The activation enthalpy of vacancies and dislocations for HPT Ni as a function of shear strain for different hydrostatic pressures. It is found that $Q(disl) = \text{const} = 0.95$ eV (filled symbols), $Q(vac) = \text{const} = 0.65$ eV (empty symbols)

Peak temperatures

A good indicator for the reliability of measured activation enthalpy data are the annealing temperatures T_{max} of the peaks observed. Both, Q and T_{max} should show similar behavior as a function of the deformation and the pressure. According to Fig. 4.15 the peak temperatures T_{max} of the only peak in Cu (representing the annealing of vacancy agglomerates and dislocations) shift to lower temperatures up to strain values below $\gamma_T = 15$, and beyond that value they level out and/or tend to shift back to higher temperatures. With all pressures applied, the same behavior is seen in the strain dependence of the related activation enthalpy $Q(disl)$ (see Fig. 4.12) so that the values of $Q(disl)$ at least for the lowest pressure 2 GPa applied, and also their strain dependence can be taken for serious. Regarding the dependence of Q on pressure, however, the activation enthalpies behave in a different way than the peak temperatures. Since the accuracy of peak temperature data is much higher than that of activation enthalpy data, one should trust in the T_{max} values rather than in the Q values.

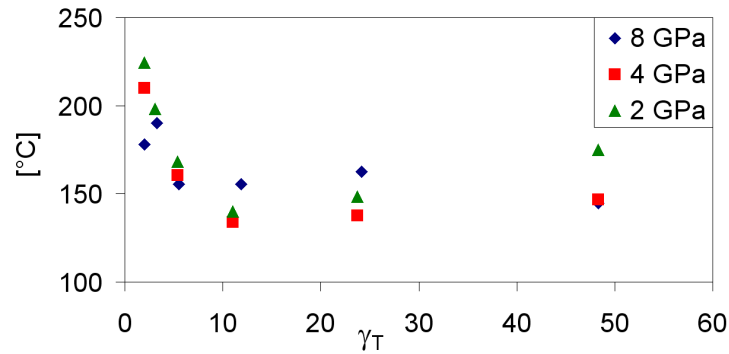


Figure 4.15: Evolution of the DSC peak temperatures of HPT Cu with increasing strain for different pressures

The strain dependences of peak temperatures of HPT Ni are shown in Fig. 4.16 for different peak types and purities. There is agreement between the peak temperature and the activation enthalpy for the single/double vacancy peak showing no dependence on strain, but this is not true for the peak temperatures of the high temperature peak at least for strains smaller than $\gamma_T = 15$ which exhibit a clear dependence on strain similar to the case of Cu. Apart from the reasons given above for the smaller reliability of Q analysis, it is evident that the high temperature peak represents the annealing of both vacancy agglomerates and dislocations, and in the Kissinger analysis only an average Q value can be evaluated with its strain dependence being suppressed.

Interpretation of activation enthalpies, and comparison with literature

The activation enthalpies measured in this work for Cu are in the range of $Q = 0.48$ to 0.78 eV, depending on the strain and pressure applied. These results are a little below the activation enthalpy of boundary migration in Cu ($Q = 1.1$ eV) found in the literature [71]. This enthalpy is also called “activation enthalpy of primary recrystallization” [38]; it represents the annihilation enthalpy of dislocations and amounts to about one half of the self diffusion enthalpy. The dependence of Q with increasing strain, and the absolute values of Q correspond well with mea-

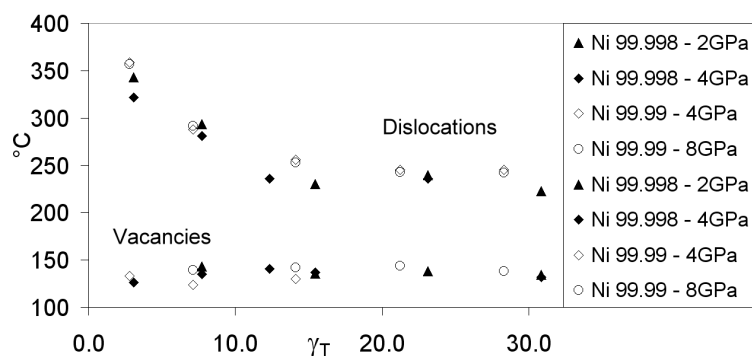


Figure 4.16: The evolution of the DSC peak temperatures as a function of strain for Ni of different purities. Note the different strain dependences of the vacancy peak, and the vacancy agglomerate/dislocation peak, respectively!

sured data from literature on Cu samples deformed by ECAP ($Q = 1$ to 0.65 eV) [69, 72] and cold rolling ($Q = 1.1$ to 0.8 eV) [73, 74]. Recent measurements of the activation enthalpy with tracer diffusion led to similar results ($Q = 0.99$ eV after one ECAP pass down to $Q = 0.67$ eV after 12 passes) [75, 76]. As for Ni, the results for activation enthalpies are also in good agreement with results from the literature [55, 77].

There has not been measured any dependence of Q on shear strain, but we should consider some, according to the peak temperature dependence for purposes of interpretation (see next section). The value of the activation enthalpy determined for Ni for single/double vacancies equals to $Q = 0.65$ eV. This is about a factor of two lower than that of vacancy bulk migration $Q = 1.18$ eV [38], which hints at the fact that single/double vacancies move by core diffusion [46, 47]. The enthalpy for primary recrystallization in Ni amounts to about 1.4 eV. Similarly as in case of Cu, the values for Ni derived by Kissinger analysis are below that of primary recrystallization. The reason for that may arise from the fact that at least in the HPT Ni with high shear strains ([S1][22], Figure 4.18), and in Cu [S1] with all strains, the high temperature peak is not only represented

by the annealing of dislocations but also by that of vacancy agglomerates which are expected to reveal a smaller activation enthalpy.

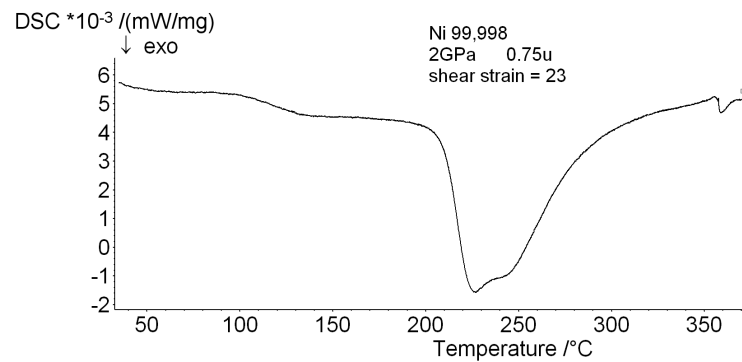


Figure 4.17: A DSC heat flow curve for Ni HPT deformed at 2 GPa to a shear strain of 23. Vacancy agglomerates and dislocations anneal at about 250°C causing an overlap of both peaks

There is no correlation of the peak temperatures and the activation enthalpies with respect to different applied pressures in both Cu and Ni. Again, the sensitivity of the Kissinger method seems to be too low in order to distinguish between the two different defect types if they contribute to only one annealing peak. The more reliable variation of the peak temperature with varying pressure in Cu is small and suggests a similarly weak dependence for the activation enthalpy of dislocation/agglomerate annihilation.

The Strain Dependence of Q : Vacancy induced vs. Stress induced annihilation of dislocations

Strain dependence of Q due to excess vacancy boosting. As has been already argued by Cao and co-workers in [72], one explanation of the decrease of Q with increasing strain could be the deformation induced formation of excessive concentration of vacancy agglomerates which is increasing with increasing shear

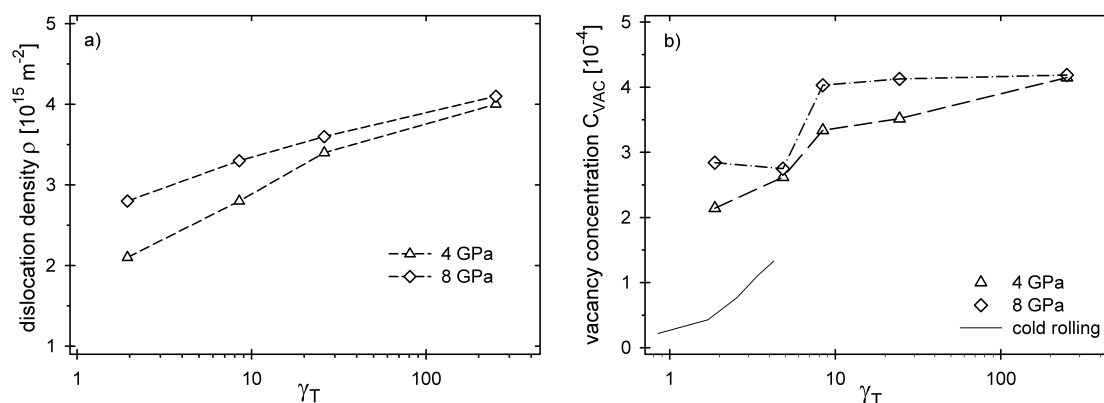


Figure 4.18:

- Dislocation densities of HPT Cu for selected γ_T as obtained by the MWP-fitting procedure
- Vacancy concentration in HPT Cu as evaluated from the difference of stored energies derived from DSC and XPA measurements [18]

strain. As already mentioned in the experimental section, XPA was used to separate the contribution of vacancy agglomerates from that of dislocations in the DSC peak for Cu: We calculated the stored energy which corresponds to the measured dislocation density shown in Fig. 4.18 a), and subtracted this value from the total stored energy measured with DSC. The remaining energy represents the stored energy of vacancy agglomerates with a diameter smaller than about 5 nm and allows for the evaluation of their concentration Fig. 4.18 b) [S1][18, 22]. The results shown in Figure 4.18 indicate that an excessive density of vacancy agglomerates is present which even increases with increasing shear strain applied. It may increasingly reduce the formation enthalpy and thus the total enthalpy of primary recrystallization. However, due to the constancy of vacancy concentration with highest applied strains (Fig. 4.18 b), this interpretation can explain a saturation of primary recrystallization enthalpy but not its

re-increase as it has been reliably measured for Cu at highest strains observed (Figs 4.12 and 4.15).

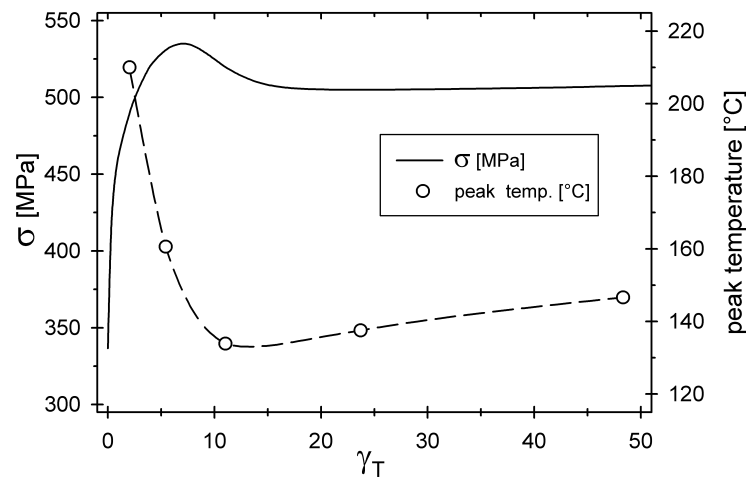


Figure 4.19: The peak temperatures measured by DSC compared with micro hardness (HV) measurements ($\sigma = HV/3$) from [67] for HPT Cu deformed at 4 GPa

Strain dependence of Q due to assistance of long range internal stress. In a previous paper of our group, measurements of the annealing temperatures T_{max} of the dislocation peak in cold rolled Cu and Al as a function of rolling strain revealed strong parallelities with the strength characteristics over the whole range of strains observed [65]. This finding was the basis to quote the presence long range internal stresses (as a part of the external ones) as a reason for the shift of T_{max} (and thus also the related activation enthalpy Q) with varying strain. Now this result led us to plot T_{max} as a function of shear strain also in case of presently studied HPT deformed Cu. Obviously the same parallelity of strain dependences of T_{max} and external stress turned out, as is demonstrated by Fig. 4.19 for a pressure of 4 GPa (similar correlations have been also found for 2 GPa

and 8 GPa). Even more direct evidence for the strain dependent change of long range internal stresses comes from previous X-ray profile analyses which are shown in Fig. 4.20 (from [67]): The higher is the shear strain accumulated, the higher is the level of internal stresses in parallel to that of the external ones. From a critical shear strain reached, the micro structure starts to recover after HPT. Thus it exhibits less and less internal stresses because of rearrangement of dislocations, and the dislocation need more and more activation enthalpy to get annihilated.

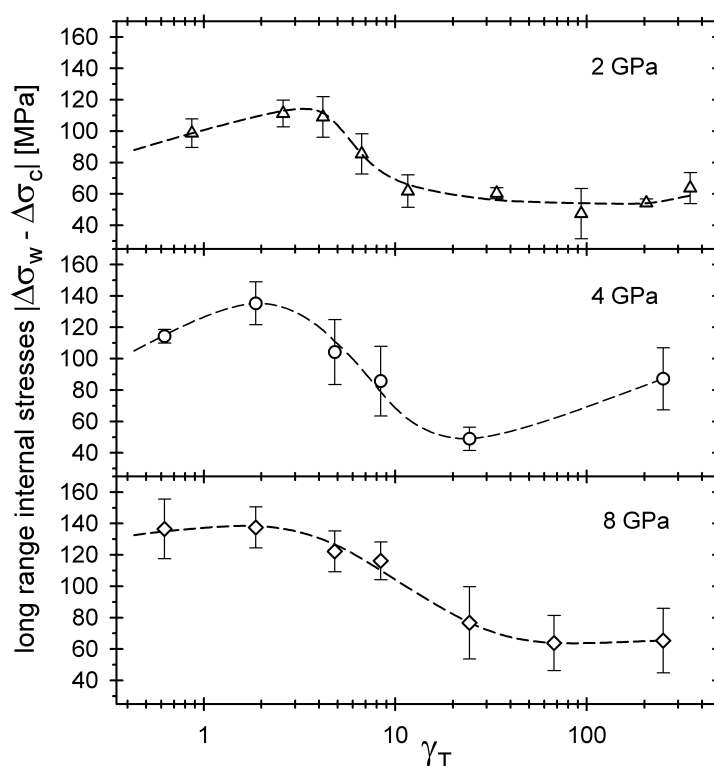


Figure 4.20: internal stresses as measured by X-ray Profile Analysis [67]

Comparing now the interpretation of vacancy boosting with that of internal stress assistance, we favor the latter because, as already mentioned, the vacancy

hypothesis cannot explain the re-increase of Q (and/or T_{max}) which occurs in Cu at very high strains. Furthermore, there has been supports by recent publications. One is by Molodova et al. [69] which explains the decrease of the activation enthalpy for Cu with increasing number of ECAP passes by the increasing ease of nucleation of grains. Further support comes from recently published works on tracer diffusion in ECAP processed materials [75, 76] which explain the lowering of Q with increasing strain by the increasing number of non-equilibrium grain boundaries. Because these non-equilibrium grain boundaries involve long range internal stresses, those findings are strictly in line with our interpretation that long range internal stresses are responsible for the strain dependence of primary recrystallization enthalpy.

4.3.4 Summary

Differential scanning calorimetry in combination with the Kissinger method has proven as an easy and fast technique for measuring defect activation enthalpies. The results of the activation enthalpies measurements in HPT deformed fcc metals Cu and Ni suggest that the annealing of HPT induced vacancies is ruled by core diffusion of vacancies, and that the annealing of HPT induced vacancy agglomerates and/or dislocations is essentially assisted by long range internal stresses. Problems with the determination of activation enthalpy arise when the annealing temperatures of different types of lattice defects comes close or even coincide. This may have been one reason why the small dependence of the activation enthalpy on the hydrostatic pressure could not be quantitatively evaluated.

4.4 Lattice Defects in Hydrogenated and HPT Processed Pd [S3]

4.4.1 Introduction

There is a number of features that can be achieved by materials processed by Severe Plastic Deformation (SPD) only, i.e. not by otherwise processed nanomaterials. These are (i) a considerable ductility, (ii) changes in phase stability, and (iii) enhancement in diffusion. Comparing the nanostructures of SPD-nanomaterials with those achieved by other methods it has been shown that deformation-induced lattice defects, especially vacancy type ones, are specific of SPD and thus predestined to explain features (i)-(iii) [4, 22]. Due to these beneficial features, there is any reason to increase the stability of vacancy type defects. One possibility is to introduce alloying atoms in the material which can act as traps for deformation induced vacancies [17]. In related literature it has been shown that hydrogen could play the role of an alloying element i.e. stabilize the vacancies [30, 31] in such high concentrations that even an ordered vacancy sublattice will form [41, 42].

It was the aim of the present work to select a metal with potential for hydrogen storage and to deform it by SPD before and after hydrogenisation. For this purpose HPT deformation on pure and hydrogenated Pd has been achieved and the number of nature of SPD induced defects - namely vacancy type ones - have been studied by means of differential scanning calorimetry. This method revealed as a suitable tool for determining the concentration of these vacancy-type defects and their activation enthalpy [S1] [4, 22, 55]. The results will be discussed and compared with our previous studies on Cu and Ni [S1] [4, 22] and those of literature [55, 78, 79].

4.4.2 Experiments

Samples and treatment

Rods of Pd with 99.95% purity were cut into disks of 6mm diameter and 0.8mm thickness using spark erosion, subsequently cleaned by sandblasting and annealed at 1073K for 2h in ultra high vacuum. Afterward the samples were loaded in a Sieverts-type apparatus with gaseous hydrogen of concentration $x = 0.6$ (0.6 hydrogen atoms per 1 Pd atom). Special loading conditions slightly above the two-phase region were chosen to avoid internal stresses (Fig. 4.21). Then the samples were deformed by HPT using the equipment at ESI Leoben, Austria [37]. By applying a hydrostatic pressure of 8GPa, shear strains of $\gamma_T = 90$ to 900 were achieved, with $\gamma_T = r\phi/d$ where r is the radius and d the thickness of the sample after deformation, the angle of rotation by the HPT process in radiant. Compressive strains resulting from pressure application could be kept smaller than 20%. The true strain is being calculated as $\epsilon = \gamma_T M_t / M_c$, with $M_t = 1.65$ and $M_c = 3.06$ as the Taylor factors of fcc metals for torsion and compression, respectively. To avoid desorption of hydrogen at room temperature, the samples were stored under liquid nitrogen before and after HPT treatment. During HPT processing they were cooled with solid CO₂ ensuring in deformation temperature of 233K.

Method - Differential calorimetry

Differential Scanning Calorimetry (DSC) measurements were performed using a Netzsch DSC 204 calorimeter operated with liquid nitrogen at a constant heating rate of 5 K/min in a temperature range from 173K to 873K. The low heating rate was chosen for comparison with literature [80]. To reach the high calorimetric accuracy in determination of the stored energy of less than 1% of peak area a reference sample of annealed Pd with equal sample mass was used. To avoid water condensation during attaching of the cooled sample into the DSC a

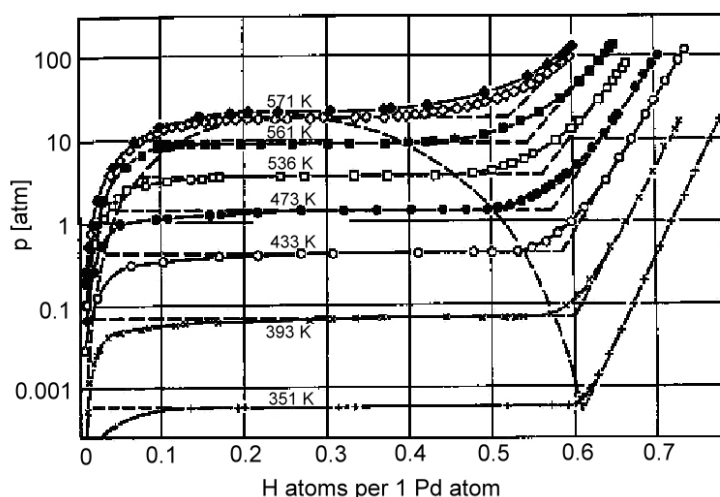


Figure 4.21: Pressure-concentration isotherms of the system Pd-H at different temperatures, including the critical two phase region [40]

self-made glove box was installed. During DSC measurements the annealing of deformation induced defects could be observed by the occurrence of exothermic peaks [S1]. The area of the peaks corresponds to the total enthalpy of annealing defects and allows to derive the density of the defects (see below). Information on the nature of the defects can be obtained from the peak temperature and the activation enthalpy [S1]. The stored energy of dislocations can be related to their density N as follows:

$$E_{stor} = Gb^2 \frac{N}{4\pi\kappa} \ln((b\sqrt{N})^{-1}) \quad (4.4)$$

where G denotes the shear modulus and b the absolute value of the Burgers vector. κ amounts to the arithmetic average of 1 and $(1 - \nu)$, with $\nu = 0.343$ as the Poisson ratio, assuming equal parts of edge and screw dislocations. The concentration of single vacancies can be evaluated from the stored energy of vacancies divided by their formation energy ΔH_v^f . In Pd $\Delta H_v^f = 1.85$ eV per single vacancy [38].

4.4.3 Results and Discussion

The similarity of basic properties of Pd and Ni allows direct comparison of results of both metals [S1]: (i) both are fcc metals; (ii) the melting temperature of Pd (1828 K) is only slightly higher than that of Ni (1728 K); (iii) the stacking fault energies for Pd and for Ni [33] are comparable and (iv) the formation energy of vacancies for palladium (Pd) = 1.85 eV and for nickel (Ni) = 1.79 eV [38] are very similar. HPT deformed Pd samples show two exothermic peaks (Fig. 4.22): the first one appears at about 373 K with an area of 0.05 J/g. This temperature corresponds to the annealing of single and/or double vacancies in deformed Pd [79]. The second peak between 523 K and 553 K is much broader than the first one because it consists of at least two single, overlapping peaks. Compared with the results from literature [S1] [78, 79] these sub-peaks could be identified as annealing of vacancy clusters and of dislocations although the area of the whole second peak is surprisingly low: For comparison the area of this peak in Ni is about 10 times higher [S1].

Compared to Pd cold rolled (CR) to a true strain of $\epsilon = 1.01$, the deformation reached in HPT samples is very high. Deformations of 6 and 30 rotations are equivalent to $\epsilon = 76$ and even $\epsilon = 380(!)$, respectively. Surprisingly, there is almost no difference in the stored energy between the cold rolled sample to $\epsilon = 1.01$ and the HPT deformed one achieving $\epsilon = 76$. Although the dislocation peak in the case of the HPT Pd is slightly shifted to lower temperature (522 K) but the total amount of energy of deformation induced defects is increased by only 0.02 J/g. Another interesting behavior is shown by the curve of the sample deformed to $\epsilon = 380$ (dashed line in Fig. 4.22). Although after deformation beyond $\epsilon = 25$ a saturation in defect concentration is to be expected, Pd seems to store an increasing density of defects even beyond deformations of $\epsilon = 76$. The DSC curve of the sample deformed up to $\epsilon = 380$ shows a peak at 561 K with an about two

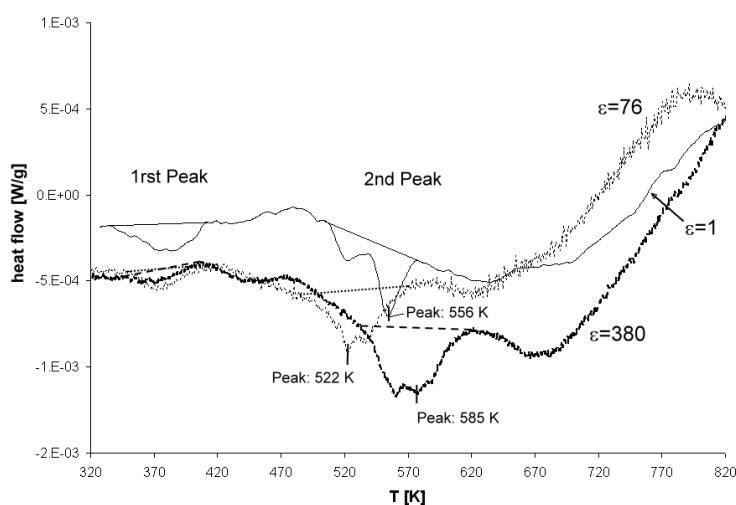


Figure 4.22: DSC results of cold rolled Pd compared to HPT (8 GPa) deformed one without H₂:

$\epsilon = 380$ - dashed line; $\epsilon = 76$ - dotted line; CR $\epsilon = 1.01$ - solid line

times higher stored energy. The higher annealing temperature indicates that the deformation defects are even more stable which somewhat contrasts the observation in other pure metals [S1]. Results of DSC measurements of hydrogenated and subsequently HPT deformed Pd (dashed line) as well as of undeformed but hydrogenated Pd (solid line; in what follows, we call it "Pd-H") are presented in Fig. 4.23. It can be seen that the DSC peaks caused by the desorption of hydrogen are different to those of annealing of lattice defects: The desorption of hydrogen is an endothermic process and releases about 100 times more energy. The areas of the two peaks shown in Fig. 4.23 are quite similar which proves that no hydrogen was lost during preparation and deformation of Pd-H. Probably due to refined grain structure caused by HPT deformation, desorption of hydrogen in HPT processed sample occurs at an about 35 K lower temperature with respect to the undeformed one. An interesting shoulder appears on the right side of the peak at about 473 K which will be discussed below. The shape of the left shoulder (313 K and 353 K) is reproducible but could not be explained so far.

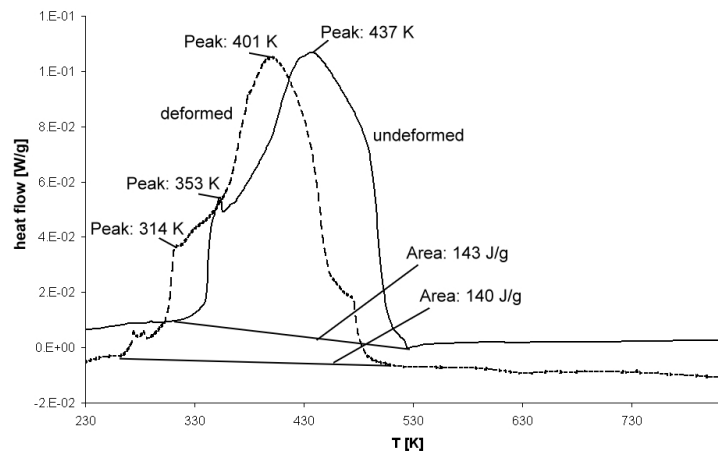


Figure 4.23: DSC results of hydrogenated undeformed Pd (solid line) compared to HPT Pd deformed by $\epsilon = 380$ at 8 GPa (dashed line)

In order to determine the small exothermic peaks of defect annealing, hydrogen loaded samples were stored at room temperature for several weeks in order to entirely desorb the hydrogen. In Fig. 4.24, DSC curves of a hydrogenated HPT deformed Pd sample (dashed line), and a HPT deformed non-hydrogenated one (solid line) are shown. For the Pd-H sample, a very sharp peak at 482 K with an area of 1.2 J/g was measured. This peak appears to correspond to annealing of hydrogen-vacancy clusters, with up to 6 hydrogen atoms around a vacancy [42, 80]. After desorption of most of the hydrogen it seems that these hydrogen trapped single vacancies are surprisingly stable and anneal at 482 K instead of 373 K compared to single vacancies solely. The concentration of these hydrogen trapped single vacancies equals to a single vacancy concentration of $c_{vac} = 7.4 \cdot 10^{-4}$, which is enormous compared to vacancy concentrations of non-hydrogenated HPT deformed Pd being $c_{vac} = 3 \cdot 10^{-5}$. This sharp peak also seems to be responsible for the right exothermic shoulder of the endothermic hydrogen peak described above. The second peak of non-hydrogenated Pd is shifted from 522 K to even 670 K when the HPT sample has been loaded with hydrogen. This shows that hydrogen also may stabilize deformation induced dislocations in Pd

[30, 31]. For proving the existence and density of dislocations, X-ray line profile analyses (XPA) are planned. Furthermore, positron annihilation and neutron scattering investigations should clarify the number of vacancies in the vacancy clusters.

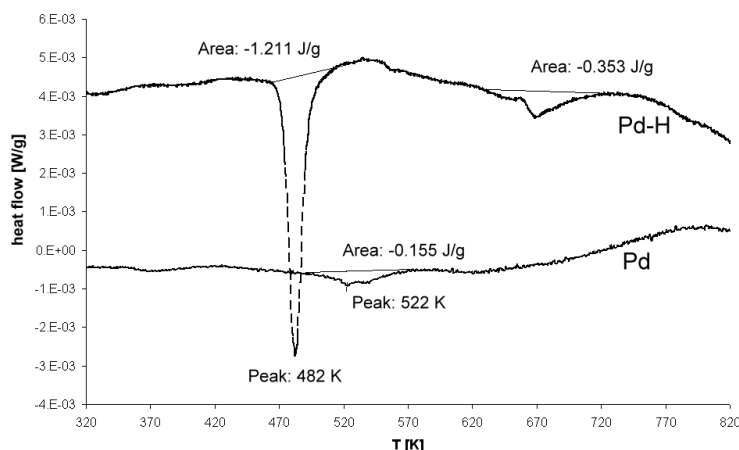


Figure 4.24: DSC results of HPT deformed Pd (8 GPa, $\epsilon = 38$): Upper curve: deformed with H; lower curve: deformed with H and annealed at RT for several weeks before DSC measurement

4.4.4 Summary

Hydrogenated and HPT-deformed Pd (99.95%) samples have been analyzed by means of differential scanning calorimetry and compared to solely HPT-deformed ones. The results can be summarized as follows:

1. Two exothermic peaks resulting from defect annealing were detected with DSC. The first one arises from vacancies while the second one is a double peak from annealing of both vacancy clusters and dislocations. The peak temperatures and stored energies correspond well to earlier results and literature, except that of the dislocation peak which indicates much lower

dislocation densities.

2. Deformation induced defects in Pd-H material anneal at much higher temperatures than those in pure Pd exhibiting an alloy effect of hydrogen in HPT deformed Pd.
3. Loading Pd samples with hydrogen and HPT processing causes a very high concentration (almost 10^{-3}) of deformation induced vacancies which is more than an order magnitude higher than without hydrogenization.
4. The high stability and number of vacancy type defects can be attributed to the formation of vacancy-hydrogen clusters.

4.5 Formation of superabundant vacancies in nano-Pd-H generated by high-pressure torsion [S4]

Since Graham's pioneering investigations in the middle of the nineteenth century [81], metal-hydrogen (M-H) systems have been studied as model alloys as, due to the rapid diffusion of hydrogen atoms in metals, solid-state reactions are generally very fast [40, 82–87]. In 1993, Fukai and his collaborators [41, 42, 48–51] observed, during in situ X-ray diffraction measurements under high hydrogen pressure and at high temperature, a gradual contraction of the lattice parameter of Ni and Pd hydrides.

Still more surprising was the fact that the reduced lattice parameter persisted after quenching to room temperature and unloading to ambient pressure. Subsequently a large number of nanopores were observed in samples subjected to additional heat treatment [48]. Instantly it became clear that their presence could not be understood either in terms of void formation in the process of hydride decomposition or simply as bubbles of hydrogen [48]. Fukai concluded that “the irreversible lattice contraction observed at high temperatures has the entire features characteristic of vacancy formation” [49]. This assumption has been proved

by observations of the formation of an ordered structure in the hydride phase [41, 42, 48–51, 80, 88] and later by investigations that revealed that the lattice contraction was in fact caused by an extraordinarily high concentration of host-metal vacancies (Vac) introduced into the hydride phase by diffusion from the surface [42, 48–51]. The vacancy concentration amounts to several atomic percent; this value is many orders of magnitudes larger than typical vacancy concentrations under ambient conditions (room temperature), and therefore the surplus vacancies were called superabundant vacancies (SAVs) [41, 42]. Since then, the phenomenon of formation of SAVs under extreme conditions has been observed in a large number of M–H systems showing various novel properties, e.g. (i) an extraordinary increase in self-diffusion coefficients [42, 52]; (ii) a drastic acceleration of foreign-atom diffusion [50, 52]; and (iii) a pronounced lowering of melting points [52]. These facts were not just attributed to SAVs but also regarded as proof of their higher thermodynamic stability compared to defect-free structures [41, 52]. Recently Kirchheim has published a model where the formation of SAVs is interpreted on the basis of thermodynamical considerations taking into account changes of the defect energy by solute segregation [31].

Later, the existence of Vac–H clusters was revealed in various electrodeposited [41, 80] and electrochemically charged metals [31, 53], as well as in thin surface films after plasma-based ion implantation [88]. These facts show that high hydrogen pressure and high temperature conditions are *not* thermodynamically necessary for SAV formation. It seems that high Vac–H concentrations have not been observed at room temperature (RT) in metals to date simply because the concentration of thermal vacancies in metals is far too low and the migration of vacancies from the surface is too sluggish. On the other hand, if SAVs are really thermodynamically stable, they should form during any process capable of introducing vacancies into the structure in sufficient number and at reasonable kinetics. Thus, a key to the problem is the so-called *deformation-induced va-*

cancies. Unfortunately, even after heavy cold work their concentration does not exceed a level of 10^{-4} [17], which is comparable to the concentration of thermal vacancies at the melting point. Higher plastic deformation is not possible due to failure of the material.

However, during the past two decades new methods of plastic deformation have been developed which are capable of processing even brittle materials – such as some hydrides – up to extremely large strains and thus allow the generation of vacancies in abundance. They are known under the generic term “severe plastic deformation” (SPD). The common principle of SPD is that samples are deformed at low homologous temperature and under high hydrostatic pressure. Of special interest from the scientific point of view is high-pressure torsion (HPT), which possesses three main advantages over all other SPD techniques: it provides (i) extremely large deformation by simple shear in (ii) a continuous way without interruption or change in strain path, under (iii) well-controlled enhanced hydrostatic pressure. The details of the technique are described elsewhere [89].

Three types of samples of high-purity Pd (99.95%, Alfa Aesar), of identical dimensions (8 mm diameter, 0.8 mm thickness) were prepared; two of them (numbered #2 and #3) were charged with hydrogen ($x_H = H/Pd = 0.78$; β phase), while sample #1 remained uncharged. Doping with hydrogen was achieved in a hydrogen gas atmosphere in a specially designed, versatile hydrogen charging device (Vienna Sieverts’ apparatus [43]) developed at the Faculty of Physics, University of Vienna. The quantity of absorbed hydrogen was calculated simultaneously during hydrogenation from Sieverts’ law and confirmed immediately after hydrogenation by the classical gravimetric method (see below). To prevent loss of hydrogen after charging, samples were forthwith frozen and stored in liquid nitrogen. Subsequently all samples were deformed by means of HPT under 8 GPa hydrostatic pressure at 265 K and at 0.2 rpm to equivalent strains $\epsilon = 42$ (samples #1 and #2) and $\epsilon = 84$ (#3), defined as

$$\epsilon = \frac{2\pi Nr}{M_{vM}d} \quad (4.5)$$

where $M_{vM} = \sqrt{3}$ (according to von Mises), N is the number of rotations, r is the radius and d is the thickness of the samples, respectively. After deformation, all samples were deposited at room temperature for 2 months in order to release interstitial hydrogen. Afterwards, a first estimation of the vacancy concentration c_{Vac} was derived from the changes in density ρ and in the lattice parameter a , according to

$$c_{Vac} = 1 - \frac{\rho_d a_d^3}{\rho_v a_v^3} \quad (4.6)$$

where the indexes v and d denote the virgin and deformed material, respectively. This equation is equivalent to the approximation of Simmons and Baluffi [90], which had been repeatedly used by Fukai [42, 51]. The density of the material was derived from high-precision measurements by gauging the difference in the buoyancy of the sample in air and in water by a slightly adapted high-sensitivity microgram balance (Sartorius M3P micro). The lattice constant was measured by routine X-ray diffraction procedures using a Bruker AXS-D8 diffractometer operated with $\text{CuK}\alpha$ radiation. With these data, the above equation allows at least the *estimation* of the total vacancy concentration, as shown in Refs. [41, 42, 51, 90]. Subsequently, differential scanning calorimetry (DSC) measurements were carried out using a Netzsch DSC 204 calorimeter in a temperature range from RT up to 775 K at a constant heating rate of 5 K min^{-1} . The transmission electron microscopy (TEM) study was carried out using a Philips CM200 on HPT-deformed Pd-H (sample #3), at first without any thermal treatment, then after a single DSC run up to 523 K and subsequently in situ heated up to 823 K. For the scanning electron microscopy (SEM) studies, the samples after DSC were *additionally* thermally treated for 1 h at 1073 K under high vacuum in

order to allow the vacancies to coalesce to pores that could be detected by SEM investigations (Zeiss Supra 40VP).

For more experimental details and DSC measurements, see Ref. [S3]. From the density method a high vacancy concentration of $6 \cdot 10^{-3}$ was estimated in pure Pd after HPT deformation (#1). This value denotes the upper limit of vacancy concentration in pure metals after SPD deformation [17, 18, 89]. Extraordinarily high total vacancy concentrations of $1.3 \cdot 10^{-2}$ and $4.8 \cdot 10^{-2}$ were found in samples #2 and #3, respectively. These values agree well with the results obtained by the density method in Pd samples exposed to high hydrogen pressure at high temperature (and containing SAVs) [42, 51] and thus provide the first proof of formation of Vac–H complexes during low-temperature SPD. However, we have to note here that, due to the poor precision of the density estimation and the low sample mass (of about 100 mg), the total accuracy of the method does not exceed $3 \cdot 10^{-3}$.

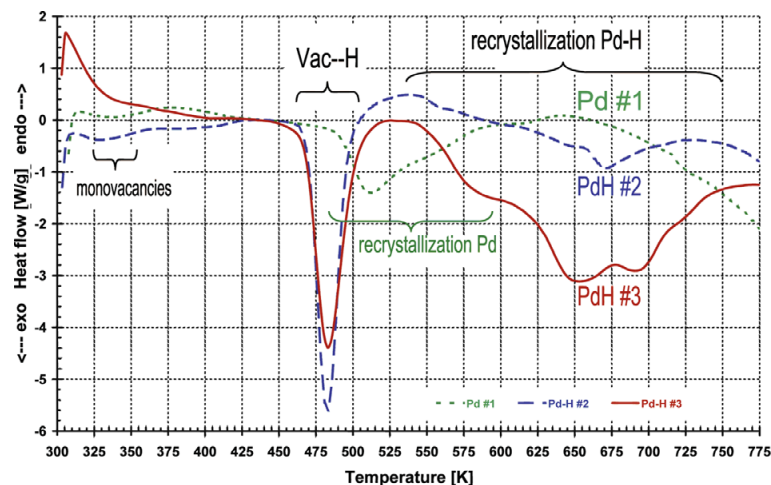


Figure 4.25: DSC curves measured on pure Pd (sample #1, dotted line) and $PdH_{0.78}$ (sample #2, dashed line), both deformed to $\epsilon = 42$, and $PdH_{0.78}$ (sample #3, full line) deformed to $\epsilon = 82$ by HPT.

The existence of Vac–H clusters was further confirmed by the DSC measurements (see Fig. 4.25 and the interpretation given below). Between 320 and 350 K a broad peak was observed in samples #1 and #2 (unfortunately, no peak could be viewed in sample #3 due to settling processes at the beginning of heating). This peak could be related to the annihilation of monovacancies [78]. From the energy released (0.1 Jg^{-1}) and the formation energy of a monovacancy in Pd (1.7 eV [40]), the same concentration of monovacancies in both samples #1 and #2 of $6.5 \cdot 10^{-5}$ was estimated. Further, in HPT-processed pure Pd (sample #1), another wide peak with 0.9 Jg^{-1} was detected between 480 and 590 K. This is attributed to the recovery and recrystallization processes, i.e. dislocation rearrangement and annihilation, in agreement with earlier results on pure Pd deformed under similar conditions [78]. In both hydrogenated samples (#2 and #3) this peak is much larger (1.7 and 3.6 Jg^{-1} , respectively), is shifted to 535 and 750 K and reflects different, overlapping recovery processes (rearrangement and annihilation of dislocations) and recrystallization, as observed in our TEM investigations (done in parallel to DSC, see below) as well as in Ref. [48].

However, far more important is the fact that a *new, pronounced* peak at 483 K was revealed in the hydrogenated and HPT-deformed samples. This is ascribed to the disintegration of vacancy–hydrogen clusters with the most stable – and therefore most probable – composition of one vacancy surrounded by six H atoms, $VacH_6$. Assuming that the total energy released (1.3 Jg^{-1}) consists of (i) the binding energy of $VacH_6$ (exothermic, 0.17 eV [40] per H atom on average), (ii) the annihilation energy of monovacancies (one per cluster, exothermic, 1.7 eV [40]) and (iii) the desorption of six interstitial hydrogen atoms (endothermic, six times (-0.1 eV) [40]), a $VacH_6$ concentration of $6.5 \cdot 10^{-4}$ was estimated in both hydrogen-charged samples. This value is in good agreement with the concentration of Vac–H clusters measured in electrodeposited [41, 80] and electrochemically charged [31, 53] metals.

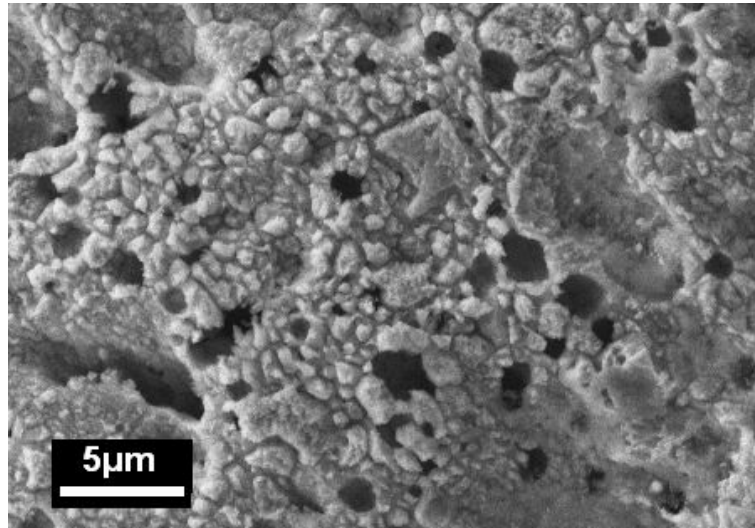


Figure 4.26: SEM picture of Pd–H after HPT and additional heat treatment showing pores of coagulated vacancies (compare to Fig. 3 in Ref. [48, 54]).

The SEM pictures in Figure 4.26 show regions with a large number of spherical voids in the hydrogenated samples #2 and #3 but not in sample #1. These regions, embedded in surrounding areas without voids, are very similar to the structure showing pores of coalesced SAVs in Ref. [48, 54]. The volume fraction of the *visible* voids corresponds to a lower bound of $8.8 \cdot 10^{-2}$ for the local vacancy concentration (in comparison to the *average* Vac–H concentration obtained from DSC above). It is worth noting that this value approaches the ideal concentration of 25 at.% in the ordered M_3Vac phase, as observed in Pd [40–42, 51].

TEM pictures reveal the microstructure of Pd–H after HPT deformation with high dislocation densities and a mean grain size of 210 ± 60 nm (Fig. 4.27a). No significant change in grain size (220 ± 95 nm) or in microstructure was observed after heating in DSC up to 523 K, i.e. above the temperature of the Vac–H peak

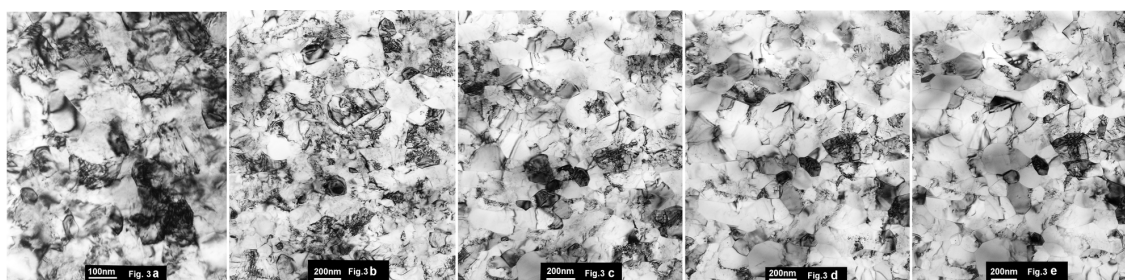


Figure 4.27: TEM images of Pd–H after (a) HPT deformation (RT, bulk); (b) HPT and one single DSC run up to 523 K (RT, bulk); (c–e) HPT, a single DSC run up to 523 K and subsequent in situ heating at 572, 673 and 723 K, respectively (thin film).

at 482 K (cf. Fig. 4.27b). These results confirm our interpretation that this peak is really related to annealing of Vac–H clusters. Further TEM images of the same sample transferred into the microscope and heated in situ up to 723 K are shown in Figure 4.27c–e. They reveal the start of recovery processes and gradual grain growth (up to 385 ± 120 nm) only just above 572 K. However, one should consider that Figure 4.27c–e shows images of a thin film whose thickness is comparable to the grain size. This could considerably hinder the grain growth.

In concluding, the results show that SAVs are generated during low-temperature plastic deformation in hydrogenated Pd, though obviously not in a homogeneous way, and Vac–H clusters coexist with deformation-induced monovacancies and with interstitial hydrogen atoms – separate release of surplus hydrogen from samples was clearly observed during storage of samples at RT. It is obvious that Vac–H clusters could only be formed from vacancies introduced into the structure by plastic deformation since, due to the low processing temperature ($0.15 T_m$), the concentration of thermal vacancies in the structure is negligible and the possibility of vacancy diffusion from the surface can also be clearly excluded.

Further, the substantial shift of the onset temperature of recovery and recrystallization towards higher temperatures by approximately 50 K may be under-

stood either (i) in terms of the existence of Vac–H clusters in the structure, which constitute active obstacles for dislocations movement, pin dislocations and grain boundaries and, consequently, impede their movement or (ii) by direct stabilizing of dislocations and grain boundaries by excess hydrogen within the same thermodynamic concept used for the vacancies [31]. The second idea is confirmed by two facts: (i) the energy released during recovery and recrystallization processes in hydrogenated Pd (#2; 1.7 Jg^{-1}) is almost two times higher compared to equally HPT deformed pure Pd (#1; 0.9 Jg^{-1}); and (ii) sample #3 released more energy during recrystallization (3.6 Jg^{-1}) than sample #2 (1.7 Jg^{-1}), suggesting that the deformation-induced dislocation density does not saturate even after such high deformations of $\epsilon = 42$ (sample #2) and $\epsilon = 82$ (sample #3), respectively.

In summary, this study demonstrates for the first time that HPT at low homologous temperature of partially hydrogenated palladium allows for the formation of Vac–H clusters even in *bulk* samples. Hitherto, this formation was only possible in powders [41, 42, 48–52] or thin layers/foils [31, 53, 54]. At RT these surplus Vac–H clusters coexist with interstitial hydrogen atoms as well as with monovacancies, and are stable in Pd up to 482 K. Results also indicate that stabilization by excess H may occur not only for vacancies but also for other deformation-induced lattice defects, namely dislocations/grain boundaries. Together, these facts show that nanometals may experience a marked increase in thermal stability through solute hydrogen.

4.6 Unpublished results

Some results which are related to the topics above were not published so far, until now. A good proof of defect stabilization by impurities is shown in Fig. 4.28. Although both Ni samples are highly pure, the difference in DSC peak temperatures between 99.99% and 99.998% Ni is obvious.

The dependence of the peak temperature on deformation degree is shown in

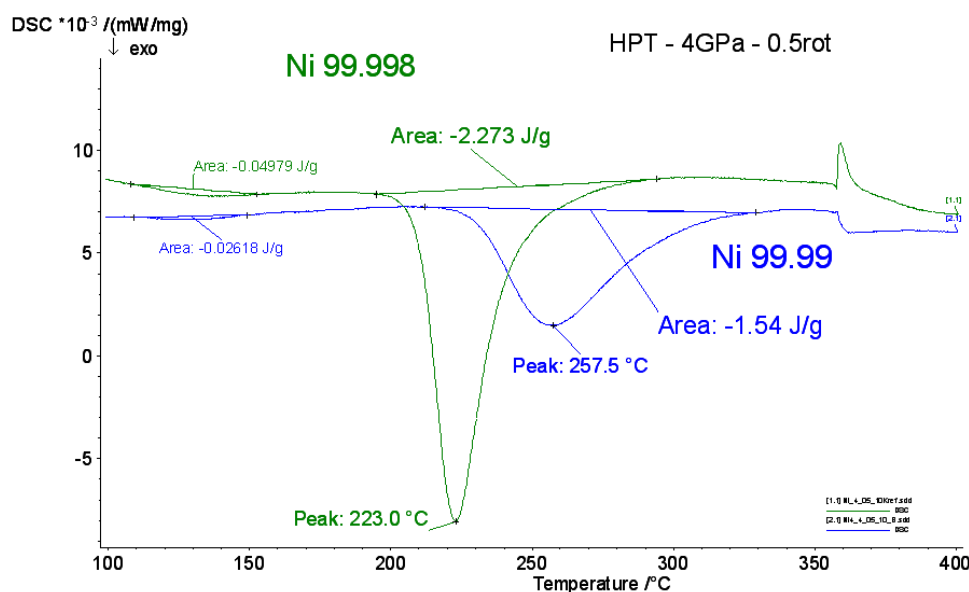


Figure 4.28: Temperature stabilization with impurities in HPT deformed Ni 99.99% compared to Ni 99.998% at 4 GPa with $\epsilon = 8$.

Fig. 4.29 in HPT deformed Ni. With increasing γ the peak temperature decreases, the peak area and so the defect density increases.

In cooperation with G. Wilde from the University Münster, Germany, tracer diffusion measurements on HPT Cu were performed in order to verify the measurements of activation enthalpy and to find out the ongoing diffusion mechanisms in HPT Cu and Ni [91]. The results fit very well with the activation enthalpy investigated by DSC see Fig. 4.30. It is interesting to note that in contrast to ECAP deformed materials, no ultrahigh diffusion could be detected which may be due to the absence of pores and microcracks in SPD samples processed with hydrostatic pressures higher than about 1.5 GPa [91].

Additional isothermal measurements helped for a better comprehension of the desorption kinetics of hydrogen loaded Pd. The mass investigation showed Fig. 4.31 that it lasts about 4 days until the interstitial hydrogen has left the metal.

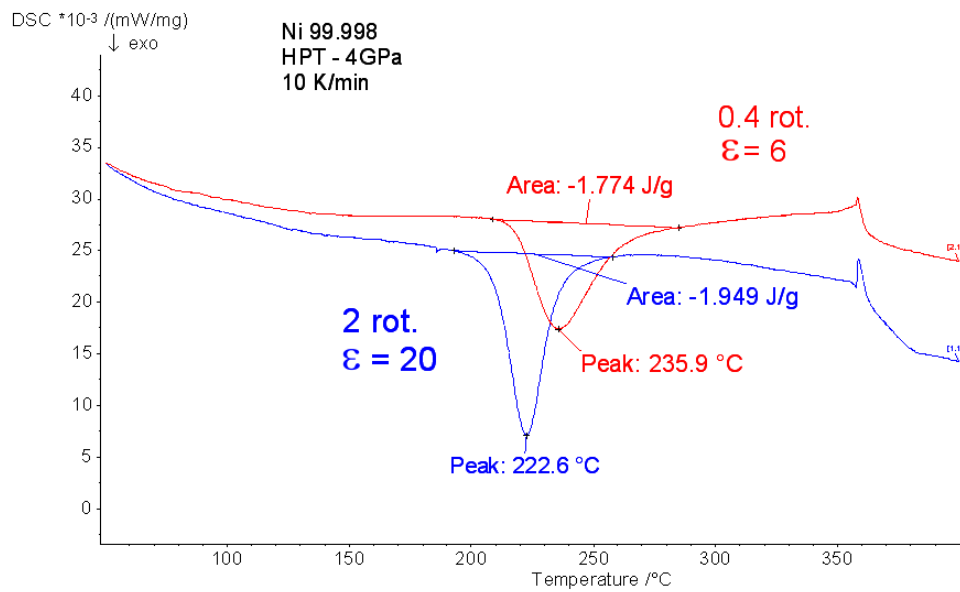


Figure 4.29: Strain dependence in HPT deformed Ni at 4 GPa.

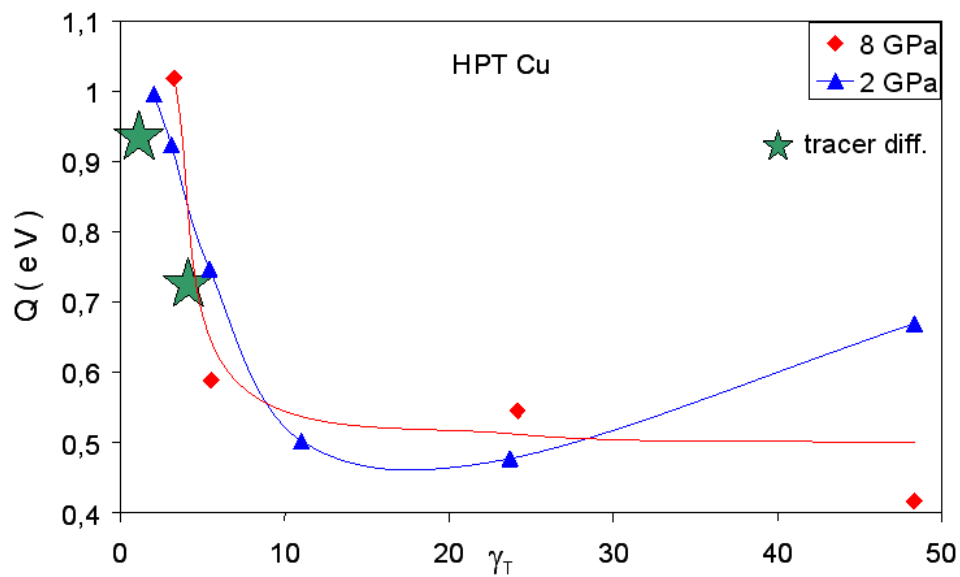


Figure 4.30: Activation energy measurements in HPT Cu performed by DSC fit very well with tracer diffusion results (stars).

During this procedure the microhardness increases by a factor of 2.5 (Fig. 4.32) which seems to indicate the formation of hydrogen vacancy clusters impeding the dislocation motion. An interesting observation was made with edges of the

microhardness indentations. Directly after loading the edges of the indentations were very clear, and after a few days slip traces and markedly bowed edges has been seen (Fig. 4.33).

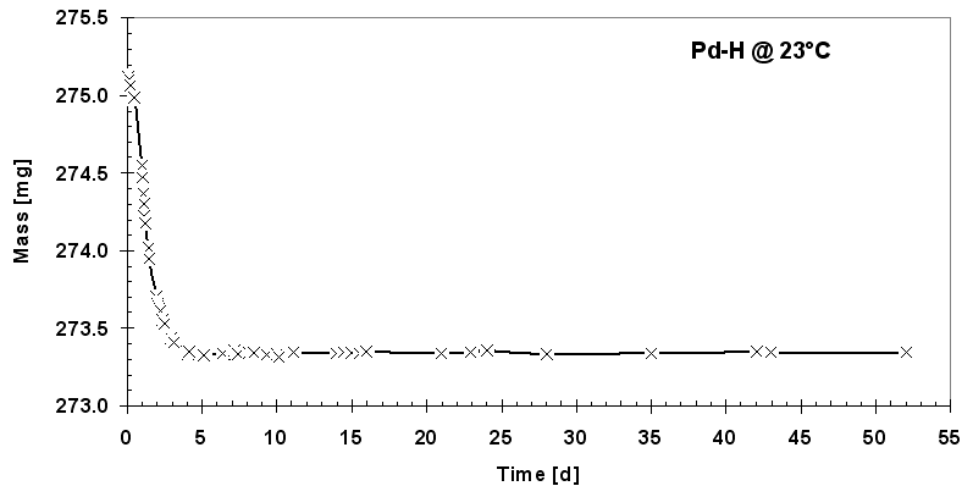


Figure 4.31: Isothermal weight measurement of hydrogen desorption at RT.

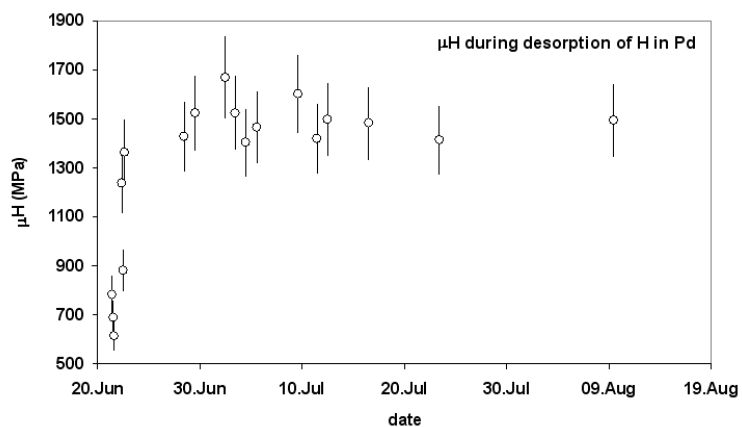


Figure 4.32: Isothermal μH measurement of hydrogen desorption at RT.

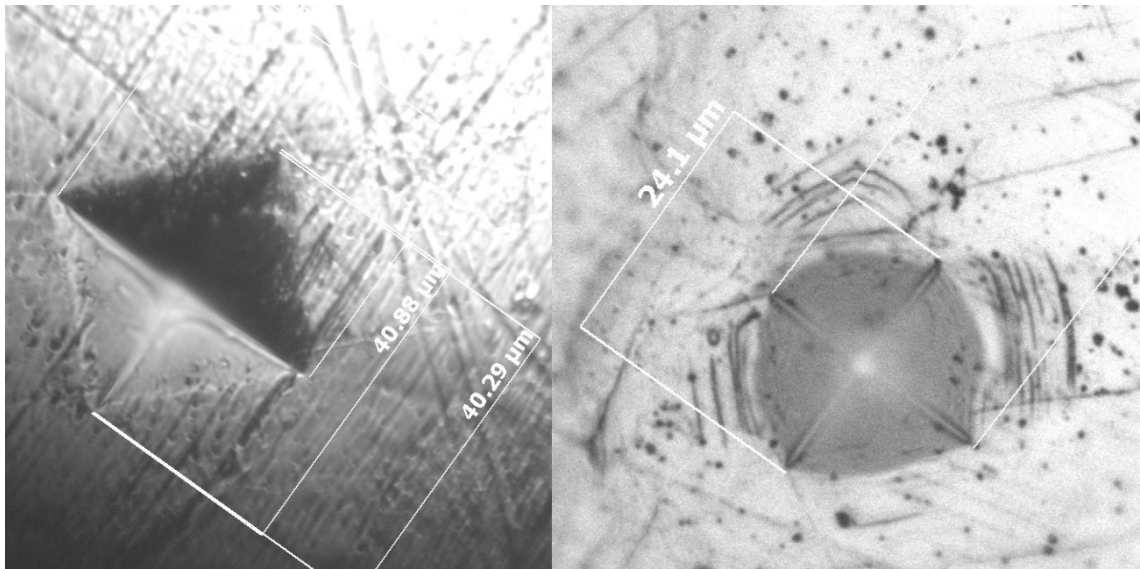


Figure 4.33: Optical micrographs of microhardness indentations directly after hydrogen loading and with visible slip traces after annealing at RT for several days.

Some additional DSC measurements were performed on HPT processed Ag (Fig. 4.34) which was chosen because of its very low stacking fault energy but still relative high mobility of defects. Like in Cu and Ni, the peak temperatures drop with increasing deformation. More investigations on Ag are in progress.

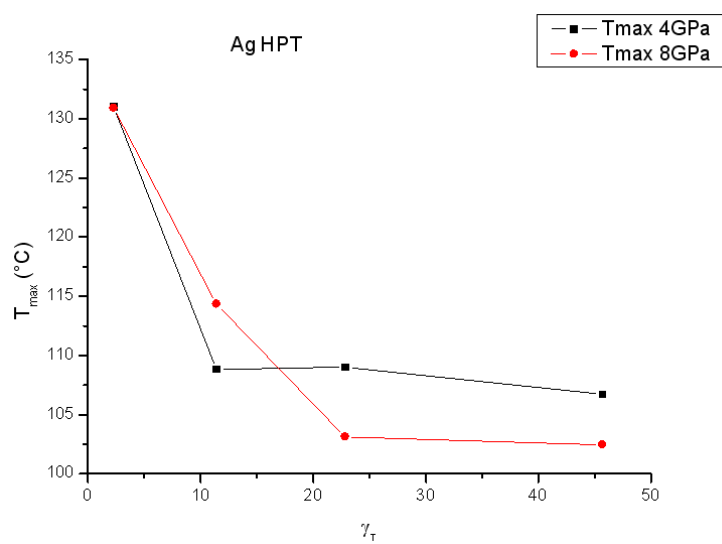


Figure 4.34: Peak temperatures of HPT deformed Ag of first DSC measurements.

Summary & Outlook

5.1 Summary

Samples of Ni, Cu and Pd were deformed by HPT (high pressure torsion) to several strains at different hydrostatic pressures. HPT was used as a representative technique for SPD nanostructures in general. The investigation of the deformation induced defects was carried out by means of DSC (differential scanning calorimetry). From the measured annealing peaks it was possible to distinguish between the defect types by different annealing temperatures and to evaluate the defect density from the peak area. Additional information was provided by the activation enthalpies connected with the annealing peaks which were determined with the Kissinger method.

In the case of *nickel*, three exothermic peaks could be detected by DSC corresponding to the annealing of single/double vacancies, vacancy agglomerates and dislocations. As the peak of vacancy agglomerates and that of dislocations have a very similar annealing temperature, the peaks related usually overlap. The

annealing temperature of the dislocation peak dropped from 350°C at the shear strain of 2 down to 250°C at the shear strain of 30. The peak temperatures of the single/double vacancy peaks are around 130°C and vary neither with strain nor pressure applied. The peak temperatures of Ni 99.99% were about 15°C higher than in Ni 99.998%. This is a clear evidence of thermal defect stabilization by impurities. The vacancy concentration measured from the peak area was in the range of 10^{-4} and thus markedly higher compared to conventionally deformed metals. The dislocation density increased from $2 \cdot 10^{15} m^{-2}$ at a shear strain of 2 to $12 \cdot 10^{15} m^{-2}$ at a shear strain of 30. In copper on the other hand only one exothermic peak of annealing of dislocations and vacancy agglomerates was present. To distinguish between dislocations and vacancy agglomerates X-ray profile analysis (XPA) was used as XPA is only sensitive to dislocations. Therefore a vacancy agglomerate concentration was determined in the range of 1 to $5 \cdot 10^{-4}$, and the dislocation density in the range of 2 to $4 \cdot 10^{15} m^{-2}$. The activation enthalpy (Q) measured in Ni for the vacancy peak is around $Q_{vac} = 0.65$ eV, and for dislocations $Q_{disl} = 0.95$ eV. In view of the differences to these values to that for vacancy bulk diffusion in Ni (1.22 eV), the value of Q_{vac} is interpreted as vacancy core diffusion while that of Q_{disl} seems to be decreased because of the presence of deformation induced vacancies. Within the actual measuring accuracy, Q neither depends on the pressure applied during deformation nor on the shear strain. Nevertheless, a slight shift of the peak annealing temperature as a function of applied shear strain could be observed.

In the case of *copper* the activation enthalpy drops from $Q = 1.0$ eV at a shear strain of about 1 down to $Q = 0.50$ eV above shear strains of 10 and remains at this value up to about a shear strain of 50. The measured results for the activation enthalpy correlate well with literature especially with recent tracer diffusion investigations. Concerning the strain dependence of the larger Q , the idea that

annihilation of dislocations is assisted by the strain-dependent concentration of vacancy type defects could not be confirmed. Rather, the annihilation of dislocations seems to be enhanced by the long-range local internal stresses because the latter exhibit very similar characteristics in strain dependence.

HPT processing have been also carried out in *hydrogenated palladium*, with the idea to generate additional deformation induced defects due to the presence of hydrogen. It could be found that indeed vacancy-hydrogen clusters have been formed during low temperature HPT and that the detection with DSC is possible. The vacancy-hydrogen cluster annealing resulted in an very sharp exothermic peak at 209°C. A very high vacancy-hydrogen concentration ($7 \cdot 10^{-4}$) was evaluated from the peak area. Dislocation densities in the hydrogenated Pd samples turned out to be by 70% higher than in Pd ones deformed without hydrogen although they are still smaller compared to other fcc metals like Ni and Cu. The identification of dislocation annealing was substantiated by specific TEM investigations, which occurs at a temperature of 400°C instead of 250°C due to hydrogen stabilization. Thus also the suspicion of the pilot paper could be confirmed that the first annealing peak did not result from dislocations but from annealing of vacancy-hydrogen clusters.

5.2 Outlook

Some work is still to do in the near future. More DSC measurements of HPT processed Ag are desirable in order to compare them with the here presented results of Cu and Ni and to better quantify the influence of stacking fault to the presence and kinetics of SPD induced defects. It is not understood that - in spite of the low stacking fault energy - the mobility of SPD produced lattice defects in Ag is very high as has been recently observed by XPA investigations within the group. Activation enthalpies are to be measured in Ag after HPT processing by different

hydrostatic pressures and to different strains, and these should be compared to the here presented results of Ni and Cu. XPA measurements should be continued to find out whether the internal stresses are responsible for the strain dependence of annealing temperature also in case of HPT Ag.

In the field of defect formation and stabilization by hydrogen more precise investigations are needed. (i) The loading conditions are to be optimized in order to reach the maximum possible defect concentration during deformation. (ii) Additional DSC investigations from H loaded Pd samples being HPT deformed to different strains, by different hydrostatic pressures at different deformation temperatures are planned. (iii) Tensile test are intended to investigate the role of high vacancy concentrations on both strength and ductility.

PhD Publications

- [S1] Setman, D., Schafler, E., Korznikova, E. & Zehetbauer, M. *Materials Science and Engineering A* **493**, 116–122 (2008)
- [S2] Setman, D., Kerber, M., Schafler, E. & Zehetbauer, M. *Metallurgical and Materials Transactions A: Physical Metallurgy and Materials Science* 1–6 (2009)
- [S3] Setman, D., Krystian, M. & Zehetbauer, M. *Materials Science Forum* **584-586**, 355–360 (2008)
- [S4] Krystian, M., Setman, D., Mingler, B., Krexner, G. & Zehetbauer, M. *Scripta Materialia* **62**, 49–52 (2010)

Bibliography

- [1] Valiev, R., Alexandrov, I., Zhu, Y. & Lowe, T. *Journal of Materials Research* **17**, 5–8 (2002)
- [2] Hebesberger, T., Stüwe, H., Vorhauer, A., Wetscher, F. & Pippan, R. *Acta Mater.* **53**, 393 (2005)
- [3] Lapovok, R., Thomson, P. F., Cottam, R. & Estrin, Y. *J. Mater. Sci.* **40**, 1699 (2005)
- [4] Schafner, E., Steiner, G., Korznikova, E., Kerber, M. & Zehetbauer, M. *Mater. Sci. Eng. A* **410-411**, 169–173 (2005)
- [5] Valiev, R., Islamgaliev, R. & Alexandrov, I. *Prog. Mater. Sci.* **45**, 103–189 (2000)
- [6] Wang, Y., Chen, M., Zhou, F. & Ma, E. *Nature* **419**, 912 (2002)
- [7] Zhu, Y., Liao, X., Srinivasan, S. & Lavernia, E. *J. Appl. Phys.* **98**, 034319 (2005)

- [8] Koch, C. *Nanostructured Materials: Processing, Properties and Potential Applications* (Noyes Publications, 2002)
- [9] Eckert, S., J. and Scudino, Yu, P. & Duhamel, C. *Materials Science Forum* **534-536**, 1405–1408 (2007)
- [10] Gleiter, H. *Acta Mater.* **48**, 1–29 (2000)
- [11] Valiev, R. & Langdon, T. *Prog. Mater. Sci.* **51**, 881–981 (2006)
- [12] Saito, Y., Utsunomiya, H., Tsui, T. & Sakai, T. *Acta Mater.* **47**, 579–583 (1999)
- [13] Tsuji, N., Saito, Y., Utsunomiya, H. & Tanigawa, S. *Scripta Mater.* **40**, 795–800 (1999)
- [14] Zhilyaev, A., Nurislamova, G., Kim, B.-K., Baró, M., Szpunar, J. & Langdon, T. *Acta Materialia* **51**, 753–765 (2003)
- [15] Gil Sevillano, J., van Houte, P. & E., A. *Prog. Mater. Sci.* **25**, 2 (1980)
- [16] Valiev, R., Estrin, Y., Horita, Z., Langdon, T., M.J., Z. & Zhu, Y. *JOM* **58**, 33–39 (2006)
- [17] Zehetbauer, M. *Key engineering materials* **97-98**, 287–306 (1994)
- [18] Zehetbauer, M., Steiner, G., Schafner, E., Korznikov, A. & Korznikova, E. *Mater. Sci. Forum* **503-504**, 57–64 (2006)
- [19] Würschum, R., Herth, S. & Brossmann, U. *Adv. Eng. Mater.* **5**, 365–372 (2003)
- [20] Würschum, R. *Mater. Sci. Forum* **363-365**, 35–39 (2001)

- [21] Sprengel, W. & Würschum, R. *Diffusion in Nanocrystalline Metallic Materials*, chap. 23, 501–517 (WILEY-VCH, 2009)
- [22] Korznikova, E., Schafler, E., Steiner, G. & Zehetbauer, M. In Publications, T. (ed.) *TMS Annual Meeting*, 97–102 (Warrendale, USA, 2006)
- [23] Zehetbauer, M., Schafler, E. & Ungár, T. *International Journal of Materials Research* **98**, 290–298 (2007)
- [24] Ungár, T. *Mater. Sci. Forum* **503-504**, 133–140 (2006)
- [25] Kocer, M., Sachslehner, F., Müller, M., Schafler, E. & Zehetbauer, M. *Mater. Sci. Forum* **210-213**, 133–140 (1996)
- [26] Oberdorfer, B. & Würschum, R. *Phys. Rev. B* **79**, 184103 (2009)
- [27] Cizek, J., Prochazka, I., Cieslar, M., Kuzel, R., Kuriplach, J., Chmelik, F., Stulikova, I., Becvar, F. & Melikhova, O. *Phys. Rev. B* **65**, 094106 (2002)
- [28] Beaver, M., Holt, D. & Titchener, A. *Prog. Mater. Sci.* **17**, 5 (1973)
- [29] Suryanarayana, C. & Koch, C. *Hyperfine Interactions* **130**, 5–44 (2000)
- [30] Kirchheim, R. Solid solutions of hydrogen in complex materials. vol. 59 of *Solid State Physics*, 203 – 291 (Academic Press, 2004)
- [31] Kirchheim, R. *Acta Materialia* **55**, 5139–5148 (2007)
- [32] Siegel, R. *J. Nucl. Mater.* **69**, 117 (1978)
- [33] Hirth, J. & Lothe, J. *Theory of Dislocations, 2nd Edn* (John Wiley&Sons, 1982)
- [34] Hull, D. & Bacon, D. *Introduction to Dislocations* (Pergamon Press, 1984)

- [35] Valiev, R. Z., Zehetbauer, M. J., Estrin, Y., Höppel, H. W., Ivanisenko, Y., Hahn, H., Wilde, G., Roven, H. J., Sauvage, X. & Langdon, T. G. *Adv.Eng.Mater.* **9**, 527–533 (2007)
- [36] Sakai, G., Nakamura, K., Horita, Z. & Langdon, T. *Materials Science and Engineering A* **406**, 268–273 (2005)
- [37] Vorhauer, A. & Pippan, R. *Scripta Mater.* **51**, 921–925 (2004)
- [38] Wollenberger, H. Point defects, ch. 17. In Cahn, R. & Haasen, P. (eds.) *Physical Metallurgy*, 1189–1221 (Elsevier, Amsterdam, 1983)
- [39] Kissinger, H. *Analytical Chemistry* **29**, 1702–1706 (1957)
- [40] Fukai, Y. *The Metal-Hydrogen System* (Springer Verlag, 1993)
- [41] Fukai, Y. *Journal of Alloys and Compounds* **356-357**, 263–269 (2003)
- [42] Fukai, Y. *Journal of Alloys and Compounds* **231**, 35–40 (1995)
- [43] Krystian, M. *Meas. Sci. Technol.* submitted (2010)
- [44] Setman, D. *Investigations of the Ordering Kinetics in Cu-48,4 at% Zn*. Master's thesis, University Vienna (2002)
- [45] Schafler, E. *Scripta Mater.* **62 (6)**, 423–426 (2010)
- [46] Sassa, K., Petry, W. & Vogl, G. *Philos Mag A* **48**, 41–61 (1983)
- [47] Canon, R. & Stark, J. *J. Appl. Phys.* **40**, 4366–4373 (1969)
- [48] Osono, H., Kino, T., Kurokawa, Y. & Fukai, Y. *J. Alloys Comp.* **231**, 41–45 (1995)
- [49] Nakamura, K. & Fukai, Y. *J. Alloys Comp.* **231**, 45–50 (1995)

- [50] Fukai, Y., Ishii, Y., Goto, Y. & Watanabe, K. *J. Alloys Comp.* **313**, 121–132 (2000)
- [51] Fukai, Y. & Okuma, N. *Phys. Rev. Lett.* **73**, 1640–1643 (1994)
- [52] Watanabe, K., Okuma, N., Fukai, Y., Sakamoto, Y. & Hayashi, Y. *Scripta Mater.* **34**, 551–557 (1996)
- [53] Cizek, J., Prochazka, I., Danis, S., Cieslar, M., Brauer, G., Anwand, W. & Kirchheim, A., R. and Pundt. *J. Alloys Comp.* **446–447**, 479–483 (2007)
- [54] dos Santos, D., Miraglia, S. & Fruchart, D. *J. Alloys Comp.* **291**, L1–L5 (1999)
- [55] Zhilyaev, A., Nurislamova, G., Surinach, S., Baro, M. & Langdon, T. *Mater. Phys. Mech.* **5**, 23–30 (2002)
- [56] Watts, B. *Dislocation in Solids*, vol. 8 (Elsevier, Amsterdam, 1989)
- [57] Warren, B. *Progress in Metal Physics* **8**, 147–202 (1959)
- [58] Ungár, T. & Borbely, A. *Appl. Phys. Lett.* **69**, 3173 (1996)
- [59] Krivoglaz, M. A. *Theory of X-ray and Thermal Neutron Scattering by Real Crystals* (Plenum Press, New York, 1996)
- [60] Wilkens, M. *Fundamental Aspects of Dislocation Theory*, vol. 2, 1195–1221 (Nat. Bur. Stand. (US) Spec. Publ. No. 317, Washington, DC, USA, 1970)
- [61] Ungár, T., Gubicza, J., Ribárik, G. & Borbely, A. *J. Appl. Cryst.* **34**, 298–310 (2001)
- [62] Ribárik, G., Ungár, T. & Gubicza, J. *J. Appl. Cryst.* **34**, 669–676 (2001)

- [63] Novak, I. Master's thesis, University of Vienna, Austria (1992)
- [64] Schafler, E., Zehetbauer, M., Kopacz, I., Ungar, T., Hanak, P., Amenitsch, H. & Bernstorff, S. *Phys. Stat. Sol. a* **175**, 501–511 (1999)
- [65] Zehetbauer, M. & Trattner, D. *Mater. Sci. and Eng.* **89**, 93–101 (1987)
- [66] Dubravina, A., Zehetbauer, M., Schafler, E. & Alexandrov, I. *Mater.Sci.Eng. A* **387–389**, 817–821 (2004)
- [67] Schafler, E., Dubravina, A., Mingler, B., Karnthaler, H. & Zehetbauer, M. *Mater. Sci. Forum* **503–504**, 51–56 (2006)
- [68] Estrin, Y., Toth, L., Brechet, Y. & Kim, H. *Mater. Sci. Forum* **503–504**, 675 (2006)
- [69] Molodova, X., Gottstein, G., Winning, M. & Hellmig, R. *Mater. Sci. Eng. A* **460-461**, 204–213 (2007)
- [70] Mughrabi, H., Ungar, T., Kienle, W. & Wilkens, M. *Philos Mag A* **53**, 793–813 (1986)
- [71] Humphreys, F. & Hatherly, M. *Recrystallization and Related Annealing Phenomena* (Pergamon Press, 2004), 2nd edn.
- [72] Cao, W., Gu, C., Pereloma, E. & Davies, C. *Mater. Sci. Eng. A* **492**, 74–79 (2008)
- [73] Meyer, U. Ph.D. thesis, Technische Universität Braunschweig (1989)
- [74] Schönborn, K. & Haessner, F. *Thermochimica Acta* **86**, 305–320 (1985)
- [75] Ribbe, J., Schmitz, G., Amouyal, Y., Estrin, Y. & Divinski, S. *Mater. Sci. Forum* **584–586**, 380–386 (2008)

- [76] Amouyal, Y., Divinski, S., Klinger, L. & Rabkin, E. *Acta Mater.* **56**, 5500–5513 (2008)
- [77] Divinski, S., Ribbe, J., Reglitz, G., Estrin, Y. & Wilde, G. *Acta Mater.* **submitted** (2009)
- [78] Würschum, R., Kübler, A., Gruss, S., Acharwaechter, P., Frank, W., Valiev, R., Mulyukov, R. & Schaefer, H. *Ann.Chim.France* **21**, 471–482 (1996)
- [79] Köster, W. & Kehrer, H. *Z. Metallkde.* **56**, 760 (1965)
- [80] Fukai, Y., Mizutani, M., Yokota, S., Kanazawa, M., Miura, Y. & Watanabe, T. *Journal of Alloys and Compounds* **356-357**, 270–273 (2003)
- [81] Graham, T. *Proc. R. Soc.* **16**, 422–427 (1968)
- [82] Schlapbach, L. E. *Hydrogen in Intermetallic Compounds I. Electronic, Thermodynamic, and Crystallographic Properties, Topics in Applied Physics*, vol. 63 (Springer, Berlin, 1988)
- [83] Schlapbach, L. E. *Hydrogen in Intermetallic Compounds II. Surface and Dynamic Properties, Applications, Topics in Applied Physics*, vol. 67 (Springer, Berlin, 1992)
- [84] Alefeld, G. & Völkl, J. E. *Hydrogen in Metals I. Basic Properties, Topics in Applied Physics*, vol. 28 (Springer, Berlin, 1987)
- [85] Alefeld, G. & Völkl, J. E. *Hydrogen in Metals II. Application-oriented Properties, Topics in Applied Physics*, vol. 29 (Springer, Berlin, 1978)
- [86] Wipf, H. *Hydrogen in Metals III. Properties and Applications* (Springer, Berlin, 1997)
- [87] Kirchheim, R. *Solid State Phys.* **59**, 203–305 (2004)

-
- [88] Semiletov, S., Baranova, R., Khodyrev, Y. & Imamov, R. *Kristallografiya* **25**, 1162–1168 (1980)
- [89] Zehetbauer, M. & Zhu, Y. E. *Bulk Nanostructured Materials* (Wiley-VCH, Weinheim, Germany, 2009)
- [90] Simmons, R. & Balluffi, R. *Phys. Rev.* **117**, 52–61 (1960)
- [91] Wilde, G., Ribbe, J., Reglitz, G., Wegner, M., Rösner, H., Estrin, Y., Zehetbauer, M., Setman, D. & S., D. *Adv. Eng. Mater.* **accepted** (2010)

Daria Setman

6.1 CV

Born on January 3th 1977 in Warsaw (Poland), living in Vienna (Austria) since 1984.

2009/04 XLPA (Xray Line Profile Analysis) school in Budapest (Hungary)

2008/07 Invitation for participation in the 58th Meeting of Nobel Laureates in Lindau (Germany)

2006/03 start with the Doctoral Thesis: "The Role of Lattice Defects in Nanocrystalline Metals Studied by Calorimetry and Resistometry"

2002-2006 Interruption of studies due to the birth and care of children (daughter Ildiko *2002/08 and son Dominik *2004/03)

2002 successful exam for the degree "Magister der Naturwissenschaften", Mag.rer.nat.

2001 Research stay at the Charles University Prague, Faculty of Physics, Czech Republic (resistivity-measurements for diploma thesis)

2001 Spring school - "Neue Materialien für die Informationstechnik" - Jülich (Germany)

2000 start with the Diploma Thesis: "Investigations of the Ordering Kinetics in Cu-48,4 at% Zn"

1996 Start of studies in "Physics" at University of Vienna

1996 Final exam "Matura" at Bundesrealgymnasium Stubenbastei Wien 1, Austria

6.2 Publications

1. "The Presence and Nature of Vacancy type Defects in SPD Nanometals" - D. Setman, E. Schafler, E. Korznikova, and M. J. Zehetbauer, Mater. Sci. Eng. A, 493 (2008) 116-122
2. "Lattice Defects in Hydrogenated and HPT Processed Pd" D. Setman, M. Krystian and M. J. Zehetbauer, Mater. Sci. Forum, 584-586 (2008) 355-360
3. "Effect of Electroplastic Deformation on Martensitic Transformation in Coarse Grained and Ultrafine Grained Ni-Ti Shape Memory Alloy" A.E. Sergeeva, D. Setman, M.J. Zehetbauer, V.V. Stolyarov and S.D. Prokoshkin, Mater. Sci. Forum, 584-586 (2008) 127-132
4. "Activation Enthalpies of deformation induced lattice defects in SPD nanometals measured by Differential Scanning Calorimetry" D. Setman, M. B. Kerber, E. Schafler and M. J. Zehetbauer, Metall. Mater. Trans. A, 41A (2010) 810-815
5. "Formation of superabundant vacancies in nano-Pd-H generated by high-pressure torsion" M. Krystian, D. Setman, B. Mingler, G. Krexner and M.J. Zehetbauer, Scripta Mater., 62 (2010) 49-52

6. "Phase evolution in rapidly solidified Al-Fe-V-Si alloys at changes of main components ratio" G. Stefanov, D. Setman, G. Avdeev, P. Kovachev and R. Petrov, Journal of Alloys and Compounds, submitted
7. "Plasticity and grain boundary diffusion at small grain sizes" G. Wilde, J. Ribbe, G. Reglitz, M. Wegner, H. Rösner, Y. Estrin, M.J. Zehetbauer, D. Setman and S. Divinski, Advanced Engineering Materials, accepted
8. "High pressure torsion induced impacts on the microstructure and physical properties of Pr_{0.67}Fe₃CoSb₁₂, Pr_{0.71}Fe_{3.5}Ni_{0.5}Sb₁₂, and Ba_{0.06}Co₄Sb₁₂" L. Zhang, A. Grytsiv, B. Bonarski, M. Kerber, D. Setman, E. Schafner, P. Rogl, E. Bauer, G. Hilscher, M. Zehetbauer, J. of All. and Comp., 494 (2010) 78-83

6.3 Conference contributions

6.3.1 Lectures

- "Properties of UFG Al-alloys after Hydroextrusion" Daria Setman, Kinga Cygan, Aug. 08, 2006, Workshop, Erich Schmid Institute of Materials Science, Austrian Academy of Science - Leoben, Austria
- "SPD lattice defects as being analyzed by annealing Calorimetry" Elena Korznikova, Daria Setman, Aug. 08, 2006, Workshop, Erich Schmid Institute of Materials Science, Austrian Academy of Science - Leoben (Austria)
- "Calorimetry of Nanocrystalline Materials" Daria Setman, Nov. 15, 2006, Lecture of IC - Vienna (Austria)
- "The Presence and Nature of Vacancy Type defects in SPD Nanometals" Daria Setman, Erhard Schafner, Elena Korznikova, and Michael J. Zehetbauer, Feb. 26, 2007, TMS 2007 - Orlando (USA)

- "Characteristics of Vacancy Type Lattice Defects in SPD Nanometals" Elena Korznikova, Daria Setman, Alexander Korznikov, Michael Kerber, Erhard Schafler and Michael J. Zehetbauer, Aug. 15, 2007, Symposium on Bulk Nanostructured Materials (BNM 2007) - Ufa (Russia)
- "Experimental Materials Science - Nanostructured Materials" Daria Setman, Jan. 16, 2008, University Vienna (Austria)
- "Calorimetric Investigations of H-Storage in HPT deformed Nanocrystalline Palladium" Daria Setman, Maciej Krystian, Jan. 31, 2008, Lecture of IC - Vienna (Austria)
- "Calorimetric Investigations of H-Storage in HPT deformed Nanocrystalline Palladium" Daria Setman, Maciej Krystian, Feb. 21, 2008, Workshop, Erich Schmid Institute of Materials Science, Austrian Academy of Science - Leoben (Austria)
- "Activation Energies of Defects in HPT Deformed Ni and Cu" Daria Setman, Apr. 30, 2008, Lecture of IC - Vienna (Austria)
- "Lattice Defects in Hydrogenated and HPT Processed Pd" Daria Setman, Maciej Krystian and Michael J. Zehetbauer, Aug. 19, 2008, nanoSPD4 Conference, Goslar (Germany)
- "Influence of Hydrostatic Pressure on Activation Energies in HPT Deformed FCC Metals" Daria Setman, Nov. 12, 2008, Lecture of IC - Vienna (Austria)
- "Migration Enthalpy investigation of deformation induced lattice defects in HPT processed Cu and Ni measured with Differential Scanning Calorimetry" Daria Setman, Michael J. Zehetbauer, Feb. 18, 2009, TMS09 Conference, San Francisco (USA)

- "Analysis of deformation induced lattice defects in SPD processed fcc nanometals by Differential Scanning Calorimetry" Daria Setman, Michael B. Kerber, Michael J. Zehetbauer, Mar. 05, 2009, NFN Meeting Planneralm (Austria)
- "Diffusion of deformation induced lattice defects in HPT processed fcc nanometals as observed by differential scanning calorimetry and radiotracer diffusion" D. Setman, S. Divinski, G. Wilde, M. Zehetbauer, Sept. 24, 2009, BNM 2009, Ufa (Russia)
- "Analysis of deformation induced lattice defects in nanocrystalline metals studied by differential scanning calorimetry" Daria Setman, Final IC Workshop, Nov. 21, 2009, Strobl (Austria)

6.3.2 Poster presentations

- "Annealing Calorimetry as a Tool for Defect Analysis in Nanometals" Elena Korznikova, Daria Setman, Erhard Schafner, Michael J. Zehetbauer, TMS 2007, Feb. 2007, Orlando (USA)
- "Effect of Electroplastic Deformation on Martensitic Transformation in Coarse Grained and Ultrafine Grained Ni-Ti Shape Memory Alloy" A.E. Sergeeva, D. Setman, M.J. Zehetbauer, V.V. Stolyarov, S.D. Prokoshkin, nanoSPD4, Aug. 2008, Goslar (Germany)
- "Analysis of deformation induced lattice defects in SPD processed fcc nanometals by Differential Scanning Calorimetry" Daria Setman, Michael B. Kerber, Michael J. Zehetbauer, TMS09, Feb. 2009, San Francisco (USA)
- "Creep - and diffusion measurements on ultrafine grained copper after high pressure torsion straining" J. Leuthold, D. Setman, M. Zehetbauer, M. Weger,

K.A. Padmanabhan, G. Wilde, BNM 2009, Sept. 2009, Ufa (Russia) - best poster presentation

6.4 Cooperations

6.4.1 Cooperations within the initiative college "Experimental Materials Science - Nanostructured Materials" IK-I022-N

Bartłomiej Bonarski: Defect analysis of HPT deformed Mg by DSC.

Johannes Koppensteiner: DMA investigations on HPT deformed Ni.

Martin Peterlechner: DSC measurements on NiTi for investigation of phase transitions and recrystallization temperature.

Lidija Rafailovics: Investigations of phase transitions in nanocrystalline FeCu and NiCo by DSC.

Florian Spieckermann: Investigations of the lamella thickness in iPP after different deformation degrees by DSC.

Long Zhang: HPT deformation of Co₃Sb nano-thermoelectrics and investigation of phase transitions by DSC.

6.4.2 National Cooperations

Abdul Ghaffar: Faculty of Physics, University Vienna (Austria): Investigations of the melting point dependence on nanopore sized Li and Na inside nanoporous Vycor with DSC.

Prof. Reinhard Pippan: ESI-ÖAW Leoben (Austria): DSC measurements of several steels (A220, P800, Fe₃Si, ...) for investigations of the influence of HPT deformation temperature on the density and stability of deformation induced defects.

Madalina Puica: Faculty of Physics, University Vienna (Austria): Check of the phase transition dependence on nanopore size of 7CB in porous Si with DSC.

Prof. Roland Würschum: TU Graz (Austria): Preparation of small samples from large HPT Cu samples for investigations of dilatation and positron annihilation. DSC measurements were carried out for comparison. Common FWF project "Freie Volumen in massiven nanokristallinen Metallen" (P21009-N20).

6.4.3 International Cooperations

Sergiy Divinsky, Gerhard Wilde: Institute of Material Physics, Univ. Münster (Germany): Tracer diffusion experiments in HPT-deformed Cu for comparison with DSC results on activation enthalpy.

Elena Korznikova, Alexander Korznikov: Institute for Metals Superplasticity Problems, Ufa (Russia): Defect analysis in HPT deformed Ni with DSC and RER.

Olga Kulyasova: Ufa State Aviation Technical University (USATU), Ufa (Russia): Phase transition dependence in HPT deformed Mg-alloys investigated by DSC.

Aleksey Podolskiy, E. Tabachnikova: B. Verkin Institute of UAS, Kharkov (Ukraine): DSC measurements concerning defect concentrations in wire-drawn and HPT deformed ultra fine grained Zr.

Anastasia Sergeeva, Vladimir Stolyarov: Mechanical Engineering Research Institute of RAS, Moscow, (Russia): DSC measurements in electro-plastically deformed NiTi.

Georgi Stefanov: Institute of Metal Science “Akad. Angel Balevski”- Bulgarian academy of sciences in Sofia (Bulgaria): Activation enthalpies of precipitation growth in Al-alloys deformed by rolling and folding were studied by DSC.

Kinga Wawer: Warsaw University of Technology (Poland): Comparison of Hydro Extruded Al-alloys with HPT deformed ones by DSC.

6.5 Teaching

Special lab course “Ordering in Alloys” SS/WS 2001 at the Faculty of Physics, University Vienna

Lab course on Material Physics “Thermal Analysis” WS 2007 - SS 2010

Lab course on basic physics (Anfängerpraktikum) SS 2008

Lab course “Fachspezifisches Praktikum - Nanomaterialien”, WS 2008 - SS 2010

Summer lab courses for pupils and students (“girls go university” and “generation innovation”) August 2009

Additional presentations in schools, kindergarten and directly at the faculty of physics (Kinderuni, Töchertag, Club Lise, FiT - Frauen in die Technik, Wissenschaftsexpress, open:physics, Schlufest, Kindergarten, ...)

Member of the mentoring program "generation innovation"

6.6 Acknowledgments

This work would not be possible without the assistance of my colleagues of the Φ nm group (Physics of Nanostructured Materials): *Christian Holzleithner, Bartek Bonarski, Florian Spieckermann, Suzi Kahofer and Jelena Horky*. It was a pleasure to work in this amicable teamwork. We were not only coworkers, we became friends. I appreciate especially the help of *Erhard Schafner* by proofreading all my publications and also the present work. To *Prof. Michael Zehetbauer* I am especially grateful for the fruitful discussions and his support as my supervisor and teacher.

I very gratefully acknowledge financial support within the PhD initiative college I-022 "Experimental Materials Science–Nanostructured Materials" and within the focus project "Bulk Nanostructured Materials", both granted by the University of Vienna, and the financial support from the FWF project P21009-N20 "Freie Volumen in massiven nanokristallinen Metallen"

Prof. Gerhard Wilde and Dr. Sergiy Divinsky I would like to thank for the very interesting cooperation in the field of tracer diffusion. I also would like to express my sincere acknowledgments to *Prof. Reinhard Pippan and Dr. Stephan Scheriau* for providing the HPT equipment and introducing me into the field of high pressure torsion. *Prof. Jürgen Eckert* I thank for the inspiring discussions and his support.

I also thank *Mrs. Regina Pinter* who helped me navigate through the paperwork jungle. I am grateful to *Dr. Gabriele Lieselotte Kerber* for the encouragement, support and the beautiful dragon. To my parents I would like to express my sincere gratitude: to my father for the self confidence and to my mother for the independence.

Finally: *Mike*, You were there for me as a colleague, friend and more . . . but most of all I thank You for Your love.

I dedicate this work to my children, *Ildiko and Dominik*, who showed me, what is truly important in life.